European Journal of Medicinal Chemistry 281 (2025) 116944

Contents lists available at ScienceDirect

European Journal of Medicinal Chemistry

journal homepage: www.elsevier.com/locate/ejmech

Research paper

A promising class of antiprotozoal agents, design and synthesis of novel Pyrimidine–Cinnamoyl hybrids

Francis Kayamba [a,b], Rajshekhar Karpoormath [a,*], Vincent A. Obakachi [a], Mavela Mahlalela [a], Danny Banda [b], Robyn L. van Zyl [c,d], Sahil Lala [c,d], Tawanda Zininga [e], Addmore Shonhai [f], Baji Baba Shaik [a], Ofentse J. Pooe [g]

[a] Department of Pharmaceutical Chemistry, Discipline of Pharmaceutical Sciences, College of Health Sciences, University of KwaZulu-Natal, Westville Campus, Durban, 4000, South Africa
[b] Department of Chemistry and Biology, School of Natural and Applied Sciences, Mulungushi University, PO Box, 80415, Kabwe, Zambia
[c] WITS Research Institute for Malaria (WRIM), Faculty of Health Sciences, University of Witwatersrand, Johannesburg, 2193, South Africa
[d] Pharmacology Division, Department of Pharmacy and Pharmacology, Faculty of Health Sciences, University of the Witwatersrand, Johannesburg, 2193, South Africa
[e] Department of Biochemistry, Stellenbosch University, Stellenbosch, 7600, South Africa
[f] Department of Biochemistry and Microbiology, Faculty of Science, Engineering and Agriculture, University of Venda, Private Bag X5050, Thohoyandou, 0950, South Africa
[g] Discipline of Biochemistry, School of Life Sciences, University of KwaZulu-Natal, Westville Campus, Durban, 4000, South Africa

ARTICLE INFO

Keywords:
Antiprotozoal activity
Malaria
Pyrimidine
Cinnamoyl group
Resistance

ABSTRACT

Malaria, caused by parasitic protozoans of the *Plasmodium* genus, continues to be one of the greatest global health crises, especially in Africa. The emergence of antimalarial drug resistance continues to be a health problem necessitating an urgent need for alternative and cost-effective antimalarials. Using a molecular hybridization approach, we report the design and synthesis of an efficacious novel class of antiprotozoal agents; (*E*)-1-(4-(4,6-diphenylpyrimidin-2-yl)piperazin-1-yl)-3-phenyl prop-2-en-1-one derivatives (**8a-r**). The *in vitro* inhibitory activity of the synthesized compounds was evaluated against the NF54 chloroquine-sensitive strain of *Plasmodium falciparum*. From the antiprotozoal screening, three compounds displayed propitious activity with IC_{50} values (0.18–0.21 μM), using quinine and chloroquine as standard antimalarials. Compounds **8o** and **8l** emerged as the most potent candidates with IC_{50} values of 0.18 ± 0.02 μM and 0.21 ± 0.001 μM with an associated good safety index of 18.59 and 16.75 to human kidney epithelial (HEK293) cells, respectively. The synthesized analogues present a new chemical architecture structurally unrelated to the current regime of antimalarial drugs, representing a valid strategy to combat resistance in *P. falciparum* species to current commercial drugs. We further investigated the binding affinities of the compounds against recombinant forms of two *P. falciparum* heat shock protein 70 homologues; PfHsp70-1 and PfHsp70-z, both of which are essential and promising druggable candidates. Compound **8l** exhibited the highest binding affinity for PfHsp70-1 and PfHsp70-z. Furthermore, molecular docking revealed that compounds **8k, 8l, 8m,** and **8o** exhibited better fitness to PfHsp70-1, with compounds **8l** and **8o** showing the highest binding affinity of −10.5 kcal/mol and −10.1 kcal/mol, respectively. Therefore, it can be speculated that PfHsp70–1 may be a possible target of some of the inhibitors tested in this study. The presence of electron-donating groups on the phenyl ring of 4,6-pyrimidine moiety and cinnamoyl group demonstrated a positive correlation between the observed computational data and the biological activity. Taken together, this paper demonstrates the importance of using the molecular hybridization approach in the development of newer cinnamoyl clubbed with 4,6-diphenyl pyrimidine hybrids as potential antiprotozoal agents.

* Corresponding author. Department of Pharmaceutical Chemistry, College of Health Sciences, University of KwaZulu Natal, Durban, 4000, South Africa.
E-mail address: karpoormath@ukzn.ac.za (R. Karpoormath).

https://doi.org/10.1016/j.ejmech.2024.116944
Received 27 December 2023; Received in revised form 21 September 2024; Accepted 4 October 2024
Available online 8 October 2024

1. Introduction

The decreased efficacy of the current first-line drugs, including artemisinin-based combination therapy (ACT), has created a global health challenge [1]. Furthermore, COVID-19 imposed restrictions stalled efforts to manage malaria, leading to more fatalities from the disease. The World Health Organization's (WHO) 2022 report on malaria indicated that malaria infections and deaths persisted despite the ongoing COVID-19 pandemic [2]. In 2021, there were an estimated 247 million cases reported with 619,000 malaria-associated deaths globally, which was a slight decline in estimated malaria deaths compared to 2020. Although there were 51,000 more deaths reported in 2022 compared to 2019 [3,4], of these cases, 76 % of the global deaths were children under the age of five and 95 % were infections from sub-Saharan Africa. Recently, the WHO recommended a new malaria vaccine, RTS,S/AS01, to be rolled out to the most affected regions, particularly children in the sub-Saharan region. RTS,S/AS01 demonstrated an overall efficacy of 36 % protection against clinical malaria and 32 % protection against severe malaria [5]; it showed 60–70 % protection in the first six months and drastically decreased to non-significance in 18 months. Drug treatment remains a viable option in managing malaria [6,7].

Medicinal chemistry, the hub that intersects chemistry and pharmacology, plays a central role in the discovery of new therapeutic agents [8]. The pursuit of designing and synthesizing small compounds with potent medicinal properties is crucial to finding new drugs.

The pyrimidine moiety is an indispensable central core in most commercial drugs due to its extensive medicinal properties, including anticancer and antimalarial properties. Our earlier studies presented a series of pyrimidine and cinnamamide hybrid analogues, which were evaluated against a panel of cancer cell lines, including chronic myeloid leukaemia (K562), acute myeloid leukaemia (MV4–11), malignant melanoma (G361), and lung adenocarcinoma (HCC827). As a result of these efforts, several potent compounds were documented, with the most potent one having a significant activity with IC_{50} values of 0.88, 1.45, 1.42, and 11.20 μM for K562, MV4-11, G361, and HCC827, respectively [9]. Regardless of these developments, there are still substantial gaps in our comprehension of the structure-activity relationships (SAR) and the potential of pyrimidine derivatives in other therapeutic areas. To further investigate the antiplasmodial activity, we expanded our investigation by employing a rational design approach to develop a 4,6-diphenylpyrimidine (depicted in Fig. 1) as a primary core structure. The quinoline was amalgamated with the pyrimidine core using an alkylene diamine linker at the second position. This class of compounds presented superior activity as antiplasmodial agents, with compound **A** (Fig. 1) being the most potent hybrid. Compound **A** displayed an IC_{50} value of 0.32 ± 0.06 μM, exhibiting a favourable safety profile of 9.79 towards mammalian cells [10] (see Fig. 2).

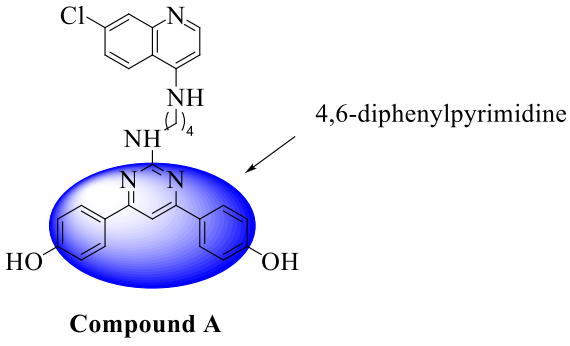

Fig. 1. The rational design of the most potent compound from our previous work [10].

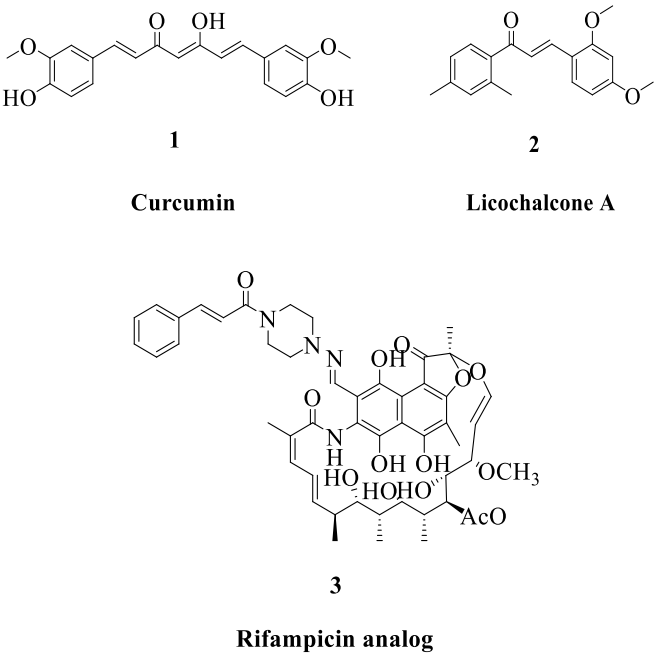

Fig. 2. Commercial drug and natural products housing a cinnamoyl core that showed antimalarial properties.

The primary objective of the current study was to synthesize novel compounds that retain the 4, 6-diphenylpyrimidine nucleus and introduce a cinnamoyl pharmacophore due to its well-established and versatile medical properties. An examination of the medicinal properties of curcumin (1), a natural compound derived from the roots of *Curcuma longa*, unequivocally confirms the presence of a cinnamoyl group in its central core pharmacophore [11,12]. Curcumin showed notable pharmacological properties such as antimicrobial [13,14], anti-inflammatory, antioxidant [15], antiproliferative, and anti-angiogenic activities [16,17]. Structurally, it possesses a cinnamoyl moiety with an enone conjugate, identified as crucial for bioactivity [18]. Additionally, curcumin has exhibited antimalarial activity against the intra-erythrocytic stages of a chloroquine-resistant malaria strain (IC_{50} value: ~5 μM), as well as inhibited 100 % *P. berghei* growth with a dose of 100 mg/kg body weight over 21 days [18]. Furthermore, a series of curcumin analogues earned patents for anti-plasmodium properties [19–21]. Licochalcone A (2), another natural compound with a cinnamoyl moiety, likewise displayed modest antiplasmodial activity (IC_{50} value: ~5 μM) [20]. The chemosensitizer-containing cinnamoyl moiety was used to evade resistance by enabling chloroquine to by-pass *P. falciparum* chloroquine resistance transporter (PfCRT), a key efflux transporter facilitating resistance [19]. The enone conjugate of chalcone (cinnamoyl moiety) was crucial in inhibiting cysteine protease, an enzyme required for haemoglobin degradation, as a source of amino acids for parasite biochemical pathways [22,23].

Rifampin is clinically used as a broad-spectrum antibiotic, mainly against *Mycobacterium*. Rifampin also exhibits significant antimalarial activity against chloroquine-resistant and -sensitive strains with IC_{50} values of 3.2 μM and 1.3 μM, respectively [24]. Rifampin housing a cinnamoyl motif essentially improved its antibiotic activity 10-fold [25]. This activity was enhanced when administered in vivo in combination with amodiaquine, where there was a significant reduction in parasitaemia and enhanced survival rate of the *P. berghei*-infected animals [26]. Rifampicin amalgamated with the cinnamoyl group when administered with amodiaquine significantly improved antimalarial activity and efficacy against *P. falciparum* [27,28].

Because of reported promising antimalarial activity displayed by numerous compounds containing cinnamoyl and pyrimidine, in our

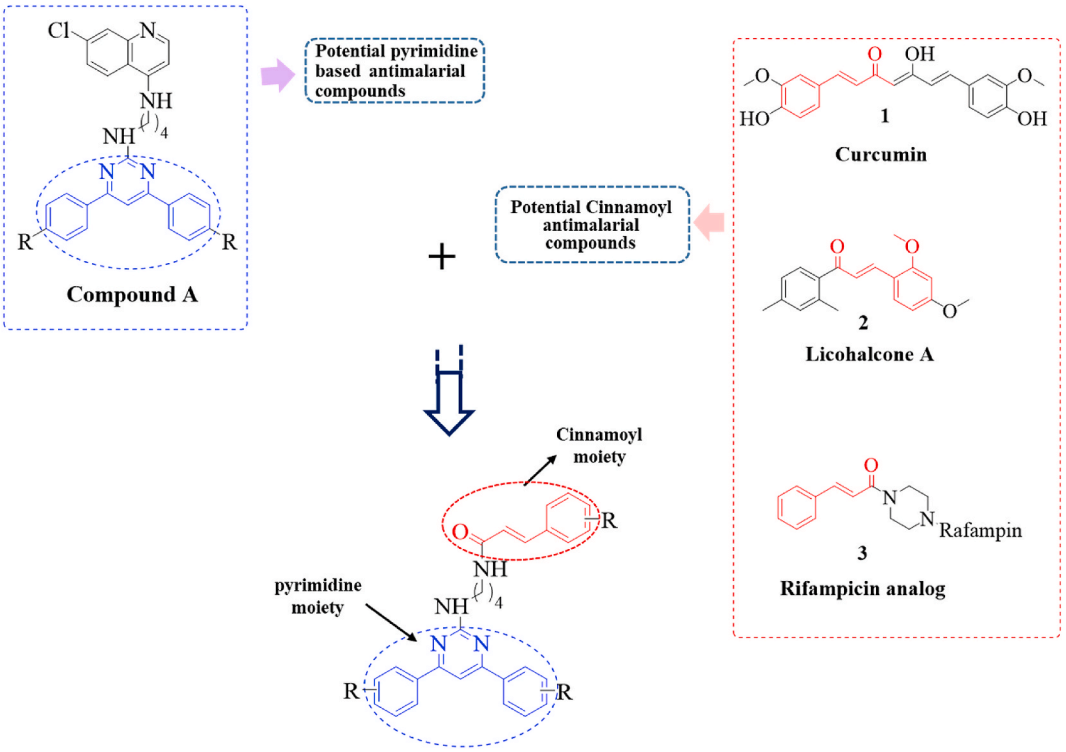

Fig. 3. Rational design of the molecular hybrid based on pyrimidine and cinnamoyl motif linked by alkylene diamine.

current study, we endeavour to further produce a 4,6-diphenylpyrimidine hybrid molecule employing the molecular hybridization approach. We conceived the hybrid molecule of cinnamoyl and pyrimidine motifs using piperazine as a linker, as depicted in the rational design in Fig. 3.

We believe that this could further enhance parasitic cell death against malaria strains of varying sensitivity profiles. Our approach seeks to deliver a single molecule with dual therapeutic action with enhanced efficacy and bioavailability [29].

2. Chemistry

The multistep synthetic route and structural elucidation of 2-chloro-4,6-diphenylpyrimidine was accomplished, as reported in our previous work [30]. Synthesis of a library of intermediates and novel cinnamoyl-pyrimidine hybrid **8(a-r)** was performed using expedient multi-step organic synthetic routes described in Schemes 1 and **2**. (*E*)-chalcones (**1**) were synthesized from assorted commercially available benzaldehydes and acetophenones by simple Aldol condensation reaction in NaOH ethanolic basic conditions as per the reported protocol [31–33]. The cyclization of assorted *(E)*-chalcones (**1**) using guanidine hydrochloride *via* NaOH basic catalyzed reaction, afforded a series of 4, 6-diphenylpyrimidin-2-amines derivatives (**2**). 2-Aminepyrimidine derivatives (**2**) were then oxidized to 4,6-diphenylpyrimidin-2-ol (**3**) by diazonium salt intermediate formation using sodium nitrate in acetic acid. Chlorination of **3** to obtain 2-chloro-4,6-diphenylpyrimidines (**4**) was completed using $POCl_3$ in catalytic DMF. Refluxing of **4** with excess piperazine in IPA yielded a series of 4,6-diphenyl-2-(piperazine-1-yl) pyrimidine (**5**), as shown in Scheme 1.

The cinnamoyl chloride (**7**) analogues were synthesized by chlorination using a versatile reagent *viz* oxalyl dichloride with catalytic DMF in DCM as in a previously reported procedure [34]. A library of the final compounds **8** (**a-r**) in good yield (73–93 %) was afforded by amidification coupling of assorted cinnamoyl chloride derivatives (**7**) and 4, 6-diphenyl-2-(piperazin-1-yl)pyrimidine (**5**) in the presence of triethylamine in DCM as illustrated in Scheme 2.

3. Results and discussion

3.1. Synthesis and spectral studies

The designed molecular structures of the final compounds coincided with the IR, ^{1}H NMR and ^{13}C- NMR spectral data obtained and HRMS for verification. The ^{1}H NMR of compound **1b** presented two discrete doublets (d) signals at δ 7.78 ppm (Ph-CH=CH) and 7.50 ppm (Ph-CH=CH) with J = 15.62 Hz and 15.61 Hz, respectively signifying the formation of an olefin with a trans conformation. The spectrum also exhibited two singlets at δ 3.89 and 2.39 ppm, indicating methoxy and methyl substituents on the diphenyl group of (*E*)-chalcone. ^{1}H NMR spectrum of compound **2** presents the appearance of two typical signals at δ 7.34 ppm and 5.22 ppm, signifying a pyrimidine aromatic proton (Pyr-H) and 2-amino group (Pyr-NH_2) of pyrimidine core and the disappearance of the olefin signals. The formation of 2-hydroxyl pyrimidine derivative (**3**) is indicated by the disappearance of the amino signal at δ 5.22 ppm and a broad singlet (br.s) signal at 11.85 ppm. The proton spectrum of 2-chloropyrimidine is characterized by the disappearance of hydroxyl (OH) signal, and minor shifts were noted for Pyr-H at δ 7.35 ppm to 7.60 ppm. 4,6-Diphenyl-2-(piperazin-1-yl)pyrimidine (**5**) ^{1}H NMR spectrum had two distinctive peaks: a broad singlet (s) at 3.93 ppm and quartet (q) at 2.57 ppm (J = 4.42 Hz) accounting for all four methylene protons of piperazinyl group. Three distinctive signals defined cinnamic acid (6) ^{1}H NMR; two doublets (d) at resonating δ 7.58 ppm (d, J = 16.05 Hz) and δ 6.55 ppm (d, J = 16.04 Hz), signifying (*E*) olefinic conformation and, broad singlet(s) at δ 12.46 ppm for carboxylic hydroxyl (OH). The ^{1}H NMR (400 and 600 MHz, DMSO-d_6) of the final compound **8c** is defined by two definite doublets (d) peaks at δ 7.74 ppm (J = 15.45) and 6.96 pp (J = 15.41 Hz), indicating the formation of (*E*) olefinic cinnamoyl group. The presence of two broad singlets (br.s) signals at δ 3.98 ppm and 3.85/3.74 ppm account for the four methylene' of piperazinyl linker, and likewise, a sharp singlet(s) signal at δ 3.85 ppm and 2.34 ppm accounting for a methoxy and methyl groups on fourth positions of diphenyl group on the pyrimidine. The outstanding protons of the aromatic group appear as diverse signals as singlets,

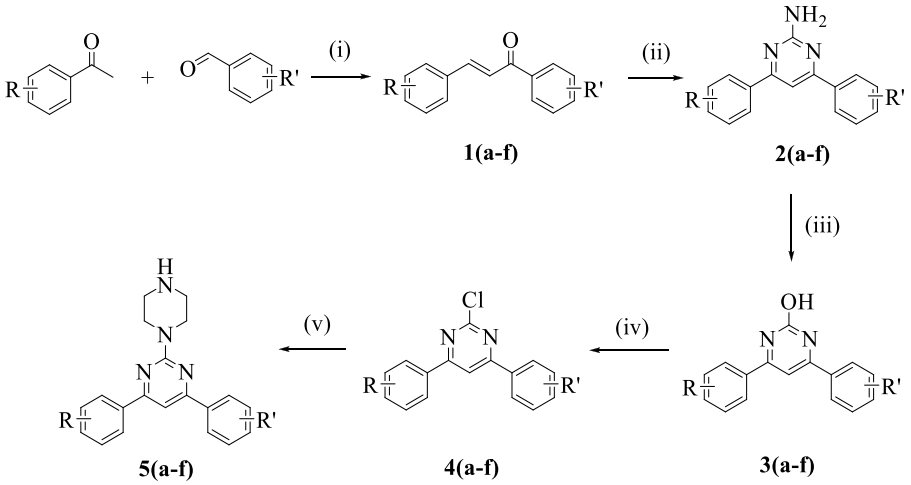

Scheme 1. Synthetic route for the intermediate **5a-f**. Reaction conditions: (i) NaOH, EtOH, rt, 2 h; (ii) Gdn.HCl, NaOH, DMF, 120 ^{O}C, 16 h; (iii) $NaNO_2$, acetic acid, rt, 3 h; (iv) $POCl_3$, DMF, 80 ^{O}C, 6 h; (v) Piperazine, IPA) 80 ^{O}C, 16 h.

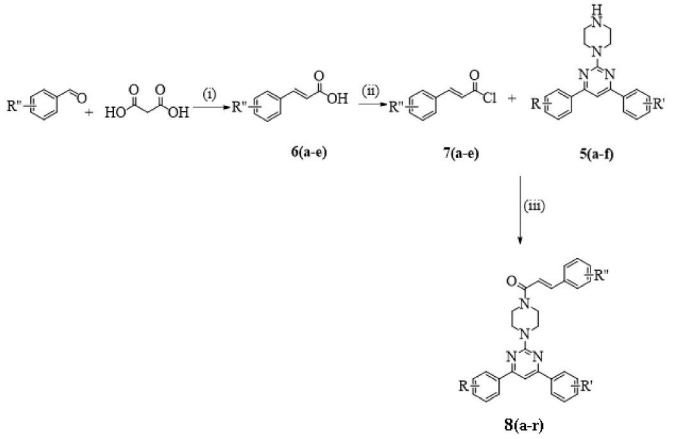

Scheme 2. Synthetic route for target novel pyrimidine–cinnamoyl hybrids. *Reaction conditions*: (i) Pyridine, piperidine, reflux, 16 h; (ii) DMF, DCM, 0 °C - rt, 1 h; (iii) Et_3N, DCM, 0 °C – rt, 3 h.

doublets, or multiples in the aromatic region (8.27 ppm–7.08 ppm). The ^{1}H NMR data of the respective compounds concurred with their corresponding ^{13}C NMR data. The most noteworthy signals resonated at δ 43.80–53.13, 55.39, and 21.44 ppm, accounting for the four methylene of piperazinyl, methoxy and methyl carbons, respectively. A distinctive signal is also observed resonating at 100 ppm, indicating a (Pyr-H) carbon. Furthermore, the characteristic signals resonated at δ 140.46 ppm, and 120.76 ppm accounted for olefinic carbons, while signals at δ 164.92–164.55 ppm and 162.12–161.54 ppm accounted for aromatic carbon-attached methoxy and (C-N). Signals resonating at 123.49–137.44 ppm accounted for the remaining aromatic carbon.

3.2. Antimalarial activity

The synthesized novel analogues of (**8a-r**) were evaluated for potent activity against the NF54 chloroquine-sensitive strain of *P. falciparum* as per the earlier reported method. The assay conditions are cited in section 13 in the supporting information. All hybrid analogues inhibited the plasmodial species, and the data obtained for **5b** and **8(a-r)** and chloroquine and quinine (standard reference drugs] are depicted in Table 1. Thirteen analogues displayed promising to moderate activity at the micromolar level against the NF54 chloroquine-sensitive strain. The IC_{50} values of these compounds were calculated from log sigmoid dose-response curves using GraphPad Prism 5.0 software (Table 1). The haemolysis assay confirmed that the analogues directed their inhibitory effect towards the intra-erythrocytic parasite and not the host red blood cell membranes. As with the standard controls, chloroquine and quinine, there was no lysis of the red blood cells, with the % haemolysis ranging from 0.01 % to 0.78 % at 50 μM of the analogues and positive controls.

Table 1
In vitro antimalarial activity of the synthesized compounds **5b** and **8a-r**.

Compound ID	Antimalarial IC_{50} (μM)	Cytotoxicity IC_{50} (μM)	Selective Index
5b	5–50	nd	nd
8a	6.02	nd	nd
8b	2.72	nd	nd
8c	1.72	nd	nd
8d	2.33	nd	nd
8e	0.60	0.93	1.54
8f	4.09	nd	nd
8g	2.71	nd	nd
8h	3.58	nd	nd
8i	5–50	nd	nd
8j	5–50	nd	nd
8k	7.43	3.69	0.50
8l	0.21	3.55	16.75
8m	0.20	0.87	4.34
8n	1.56	nd	nd
8o	0.18	3.36	18.59
8p	0.72	nd	nd
8q	3.67	nd	nd
8r	5–50	nd	nd
Quinine	0.11	134.35	1243.98
Chloroquine	0.01	101.19	8432.50
Camptothecin	nd	0.2	nd

IC_{50}: Concentration at 50 % inhibition of the parasite's growth.
Selective Index: IC_{50} values of cytotoxic activity/IC_{50} values of antimalarial activity.
nd: not done.

Out of all the evaluated compounds, **8l**, **8m** and **8o** showed the most significant antiprotozoal inhibition, with IC_{50} values below 0.5 μM corresponding to 0.21 ± 0.00 μM, 0.20 ± 0.04 μM and 0.18 ± 0.02 μM, respectively, with **8o** being the most active. Nine compounds (**8b**, **8c**, **8d**, **8e**,**8f**, **8g**, **8h**, **8p** and **8q**) displayed moderate activity with IC_{50} value (0.50–5.0 μM), while the activity of the remaining five compounds (**8a**, **8i**, **8j**, **8k** and **8r**) was considered inactive with IC_{50} greater than 5 μM. Quinine and chloroquine were two and eighteen times more active

than the most potent compounds (**8o**). This highlights the potential of these hybrids as antimalarials. Three pyrimidine-cinnamoyl hybrid compounds were considered potent, with the most active IC_{50} values as low as 0.18 μM, two-fold more active than our last reported compounds [30]. This indicates that a cinnamoyl amalgamated pyrimidine demonstrated promising activity. Also, as noted by the improved activity of these hybrids, it shows how a cinnamoyl core is significant to the antiplasmodial activity in line with the Bianca et al. report [30,35].

Since a substantial number of hybrid analogues were evaluated for their activities, a purposeful SAR to determine the members that significantly impact the respective activities of the synthesized series was undertaken. The bioisosteric substitution on the phenyl groups on the 4,6-diphenylprimidine and cinnamoyl motifs positively correlated with the antiprotozoal activity. The compounds housing a 4-(3,4-dimethoxyphenyl)-6-(4-ethylphenyl)pyrimidine motif showed promising results with IC_{50} values ranging from 0.18 to 1.56 μM. Compounds **8o**, **8i** and **8m** were the most active, with IC_{50} values less than 0.5 μM (Table 1), while compounds **8n** and **8p** showed moderate activity IC_{50} with 0.72 and 1.56 μM, respectively. Bioisosteric replacement on the cinnamoyl motif afforded a variation in the activity. An activating and a mild withdrawing group, such as methoxy and chloro, respectively, at position four of the phenyl group, showed the most activity illustrated by compounds **8m** and **8o**. Similarly, there was no observed significant difference for unsubstituted phenyl on the cinnamoyl group of compounds **8l** compared to **8m** and **8o**. However, replacing the phenyl with a heteroaromatic group, such as pyrrole, reduced the activity three-fold, as demonstrated by **8h** and **8p**. Compounds with a 4,6-bis(4-methoxyphenyl)pyrimidine core were moderate to inactive with IC_{50} values ranging from 2.71 to 7.43 μM. Here also, the bioisosteric replacements on the cinnamoyl motif presented a difference in the activity. Compounds **8f**, **8g** and **8h** displayed moderate activity with IC_{50} values ranging from 2.71 to 4.09 μM. Mild activating and withdrawal groups such as methyl and chloro induced moderate activity. Unsubstituted phenyl on the cinnamoyl also showed moderate activity with an IC_{50} value of 4.09 μM; however, substituting the phenyl group with the pyrrole group reduced the activity by about two-fold depicted by compounds **8f** and **8k**.

Compounds bearing a 4-(4-methoxyphenyl)-6-(p-tolyl)pyrimidine nucleus had IC_{50} values ranging from 0.60 to 9.02 μM. Activating and mild electron-withdrawing groups on the phenyl group of cinnamoyl core portrayed moderate activity with IC_{50} values ranging from 0.6 to 2.33, as illustrated by compounds **8c**, **8d** and **8e**. A non-substituted phenyl of the cinnamoyl group (**8b**) showed moderate activity (2.72 μM). In contrast, substituting a methyl group at the fourth position reduced activity by approximately two-fold, while dimethoxy substitutions at the third and fourth positions enhanced the activity about five times. Substitution with a mild activating group, such as methyl at the fourth position, results in an inactive compound. Replacing the phenyl with heteroaromatic compounds such as pyridine on the fourth position of the diphenylpyrimidine core did not affect the activity, as demonstrated by compounds **8a** and **8q**. It can be deduced that substitution on the phenyl of the diphenyl pyrimidine and cinnamoyl was crucial to the antiplasmodial activity.

The target stage of the intra-erythrocytic malaria parasite was determined for two of the more active analogues, namely **8l** and **8o**, as described in Section 13. It was determined that both analogues targeted the trophozoite stage, which consequently decreased the development of the schizonts and the second generation of rings (Fig. 6). With **8o** more active than **8l**, but as active as quinine at their respective IC_{50} values (Table 1).

Additionally, the cytotoxicity screening of the most potent molecules **8k, 8l, 8m, 8o** against mammalian cells was investigated to determine the selectivity of the compounds (Table 1). The selective index (SI) of the most potent compound was calculated using the IC_{50} value of the cytotoxic activity divided by IC_{50} values of antimalarial activity formulae. The SI of 0.50, 16.75, 4.34 and 18.59, corresponding to **8k**, **8l**, **8m** and **8o**, respectively, were obtained. Only compounds **8l** and **8o** displayed a good safety index, indicating a 10-fold selective inhibition of the parasite compared to the human cells.

Table 2
Relative affinities for the association of PfHsp70-1 and PfHsp70-z with compounds **8o** and **8l.**

Ligand	Analyte	*Ka* (1/M*s)	*Kd* (1/s)	K_D (M)	X^2
PfHsp70-1	**8o**	5.92 (±0.02) e^6	9.29 (±0.21) e^{-2}	1.57 (±0.7) e^{-9}	1.2
	8l	7.97 (±0.1) e^6	7.72 (±0.7) e^{-2}	9.69 (±0.5) e^{-9}	2.0
PfHsp70-z	**8o**	6.24 (±0.4) e^6	9.79 (±0.8) e^{-2}	1.57 (±0.8) e^{-8}	1.0
	8l	8.28 (±0.2) e^6	8.97 (±0.07) e^{-2}	1.08 (±0.2) e^{-8}	2.1

Standard errors of measurement are shown in parentheses.

3.2.1. *In vitro binding affinity studies*

Previously, we demonstrated that pyrimidine-based derivatives, particularly compounds **6h**, **6k**, **7a** and **7b**, have an affinity for recombinant forms of two essential chaperones of *P. falciparum*, PfHsp70-1 and PfHsp70-z [30]. As such, in the current study, we explored the direct binding of compounds **8o** and **8l** to recombinant PfHsp70-1 and PfHsp70-z using SPR analysis. Based on the sensorgrams generated, it was observed that the compounds **8o** and **8l** bound to both proteins in a concentration-dependent manner. The association of the compounds with the recombinant proteins was fast, between 5.92 and 8.28 million binding events per second, and reached saturation between **8l** and both proteins (Table 2). Compound **8o** reached saturation with PfHsp70-1 before PfHsp70-z. This suggests that there was a marginal selectivity between the association of compound 8o towards PfHsp70-1. However, there were no significant differences in the dissociation constants registered by the compound **8o** for both proteins. Based on the association and dissociation kinetics, the steady-state binding affinities of the compounds to the proteins were in the nanomolar. The compounds, **8o** and **8l,** bound to PfHsp70-1 with high affinity (in a low nanomolar range) compared to PfHsp70-z to which they bound with 10-fold less affinity (Table 2). This suggests that the compounds are biased towards PfHsp70-1 than PfHsp70-z. Since PfHsp70-1 and PfHsp70-z are homologues, the selectivity of the compounds for PfHsp70-1 as opposed to PfHsp70-z demonstrates their high precision. Overall, the compounds demonstrated significant affinities for the two proteins. Since both proteins are essential, the possible targeting of these proteins by the compounds may account for their notable antiplasmodial activities.

4. Molecular docking assessment

Molecular docking is one of the most frequently used methods in structural-based drug design because of its ability to predict the conformation of small-molecule ligands within the appropriate target binding site [36]. Hence, molecular docking assessment was performed on the four compounds that exhibited good experimental activity to study the predominant binding modes and to measure the compound's fitness at the active catalytic sites of the 3D structure of the two NBDs (PfHsp70-1 and PfHsp70-z). These four compounds were docked into the ATPase active sites of PfHsp70-1 and PfHsp70-z to calculate and examine the fitness/affinity of the compounds. The computational data obtained suggest that the compounds attach to the ATPase domain of both proteins in a manner comparable to the similar pattern ATP binds. Thereby offering the capability that these compounds could be competitive inhibitors of ATP binding for both PfHsp70-1 and PfHsp70-z. The binding modes and docking results of the compounds for each molecular chaperone are represented in Fig. 7.

Similarly, just as in our previous work [30], the four compounds, in this case, showed relatively good binding scores for PfHsp70-1 compared to PfHsp70-z. Compounds **8l** and **8m** led to the highest and lowest docking scores of −10.5 kcal/mol and −9.6 kcal/mol, respectively. At the same time, compounds **8k** and **8o** showed intermediary

scores of −9.8 kcal/mol and −10.1 kcal/mol, respectively. The docking results for PfHsp70-z revealed that compound **8l** exhibited the highest docking score of −8.3 kcal/mol while compound **8k** showed the lowest value of −7.4 kcal/mol, followed by compound **8m** with −7.9 kcal/mol. In addition, compounds **8l** and **8o** showed the highest and best binding scores in the case of the two enzymes, making them a more competitive inhibitor than others. Based on the generated data, it could be inferred that the four compounds exhibited better fitness in PfHsp70-1 than in PfHsp70-z. However, molecular docking scores may not give an apparent 100 % accuracy because standard scoring functions from molecular docking programs are still unable to discriminate binders from non-binders [37]. On the other hand, molecular dynamics (M.D.) simulation effectively incorporates the flexibility of both ligand and receptor, more accurately describes their interactions, and adds solvation effects, which more realistically depicts the protein-ligand binding process [37]. For a more in-depth understanding of the binding affinity and structural mechanisms of inhibition of the four compounds against the two enzymes, M.D. simulation analysis was investigated for the best binding modes of the compounds with the highest docking scores.

5. The binding energy/affinity of the compounds to PfHsp70-1 and PfHsp70-z

After the two protein systems undertook 100 ns of Molecular Dynamic Simulation (MDS) trajectories, Molecular Mechanics/Generalized Born Surface Area (MMGBSA) was employed to calculate the binding free energy of some of the best-docked compounds, including the four compounds (**8k, 8l, 8m** and **8o**). Only specific residues that interacted with the compounds were imputed for the calculation, and the frame period monitored was from 1000 to 40000 frames. Table 3 displays the outcome of the thermodynamic binding free energy calculation for the compounds for both enzymes. For the PfHsp70-1 complexes, the results showed that all compounds exhibited good binding energy, with compounds **8l** and **8o** possessing the highest values of **-**44.808 kcal/mol and −42.551kcam/mol, respectively. Compound **8k** exhibited higher binding energy (−40.630 kcal/mol) than **8m** (−40.500 kcal/mol) compared to the other compounds (**8a** and **8p**), with relatively good docking scores. The result validates the earlier docking results, indicating that compounds **8l** and **8o** had the highest docking score for PfHsp70-1. High van der Waals (vdW) interaction energies were observed for the four compounds (**8k**, −55.895 kcal/mol, 8l −57.431 kcal/mol, **8m**, −55.875 kcal/mol, and **8o**, −58.308 kcal/mol) compared to other compounds **8a**, −44.065 kcal/mol and **8p**, −48.080 kcal/mol suggesting their potential to be suitable inhibitors of PfHsp70-1. In the PfHsp70-z complex system, compounds **8l** and **8o** also exhibited the highest binding affinities of −36.430 kcal/mol and −35.667 kcal/mol, respectively. This is also in line with the docking result that showed compounds **8l** and **8o** with the highest docking score. From data in Table 3 on the thermodynamic binding free energy of the two protein systems, it could be inferred that PfHsp70-1 shows a more binding affinity to the compounds than PfHsp70-z. The high binding affinities indicate PfHsp70-1 as a more receptive biological target for the compounds (**8k, 8l, 8m, 8o**) than PfHsp70-z.

6. The receptor-ligand interaction profile of the compounds

Obakachi et al. (2002) used receptor-ligand interaction plots to examine the molecular interactions between amino acid residues and bound compounds [37]. Therefore, for more insightful details into the inhibitory characteristics of the four compounds, the interactions between the receptor and ligand (compounds) were examined through the plots. The plots analyze the molecular interactions between the bound compounds and the amino acid residues at the active site of an enzyme. The 2D representation of the interaction plots, as displayed in Figs. 4 and 5, shows the interactions between the compounds (**8k, 8l, 8m,** and **8o**) and the different amino acid residues of PfHsp70-1 and PfHsp70-z, respectively. Interactions such as H-bond, alkyl, amide-π stacked, π-anion, π-alkyl, π-π T-shaped, π-cation, π-π stacked and van der Waal overlap are the interactions observed in the PfHsp70-1 complexes. The interaction of compounds **8l** and **8o** with PfHsp70-1 has the highest number of interactions, 23 and 21, respectively. While those interactions of PfHsp70-1 with compounds **8m** and **8k** indicate a lower number of interactions of 16 and 17, respectively. The interaction of hydrogen bonds is critical for the inhibition of biological targets. Its importance in biological systems cannot be overstated because it aids in protein-ligand interaction and structural integrity [38]. The data on the total number of interactions and the number of H-bonds observed in the four compounds revealed that they are directly proportional to the binding energy. This could have accounted for the higher value of binding energy and inhibition status attributed to the compounds **8l** and **8o**.

We observed unique direct interactions for ligand. The number of interaction associated with compounds **8m** and **8k** are higher than those of compounds **8l** and **8o,** respectively. This could be due to the orientation and conformation of the compounds to the protein. Figs. 7 and 8 show that the interaction type unique to either protein is Pi-anion and Pi-stacked. All compounds showed significant H-bond and van der Waal interactions required for mainting protein folding and stability. The difference in the number and type of interactions observed for the two proteins NBDs (PfHsp70-1 and PfHsp70-z) could explain the higher binding energies observed in the PfHsp70-1 complexes (see Fig. 9).

Table 3
Thermodynamic binding free energy profile of the two protein systems.

	Energy Components (kcal/mol)				
Complex	ΔE_{vdW}	ΔE_{elec}	ΔG_{gas}	ΔG_{solv}	ΔG_{bind}
PfHsp70-1					
8a	−44.065 ± 4.984	−27.316 ± 6.192	−71.381 ± 8.949	37.751 ± 6.092	−33.630 ± 4.011
8k	−55.895 ± 6.499	−18.590 ± 9.938	−74.485 ± 14.564	33.573 ± 8.286	−40.912 ± 7.422
8l	−57.431 ± 5.733	−17.926 ± 7.174	−75.357 ± 10.907	30.549 ± 7.022	−44.808 ± 5.757
8m	−55.875 ± 3.734	−25.846 ± 7.081	−81.721 ± 8.262	41.221 ± 6.547	−40.500 ± 3.880
8o	−58.308 ± 6.996	−28.458 ± 11.964	−87.333 ± 12.828	44.782 ± 10.505	−42.551 ± 6.394
8p	−48.080 ± 4.792	−27.199 ± 7.317	−75.279 ± 9.370	39.785 ± 6.438	−35.494 ± 4.439
PfHsp70-z					
8d	−45.480 ± 5.967	−10.882 ± 9.650	56.362 ± 11.740	27.758 ± 7.593	−28.604 ± 5.778
8k	−41.209 ± 5.234	−12.578 ± 11.231	−53.787 ± 11.953	26.562 ± 8.126	−27.225 ± 5.161
8l	−55.812 ± 8.346	−14.206 ± 5.671	−70.019 ± 10.840	33.588 ± 5.348	−36.430 ± 8.008
8m	−40.926 ± 6.206	−22.746 ± 7.932	−63.672 ± 10.936	34.935 ± 6.422	−28.737 ± 6.173
8o	−57.451 ± 6.175	−10.028 ± 6.573	−67.480 ± 9.807	31.812 ± 6.868	−35.667 ± 4.574
8q	−30.250 ± 5.119	−12.061 ± 7.929	−42.311 ± 9.675	25.246 ± 6.664	−17.064 ± 4.706

ΔE: ele electrostatic energy, ΔE_{vdW}: van der Waals energy, ΔG: total binding free energy, $\Delta G_{sol:}$ solvation free energy, ΔE_{gas}: gas-phase free energy.

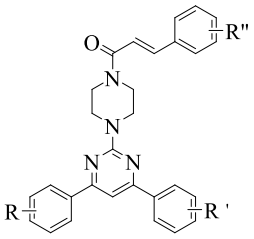

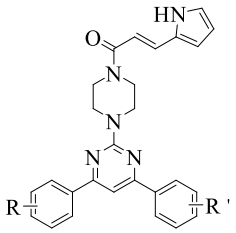

8a R = 4-Cl, R' = 4-MeO, R" = H
8b R = 4-Me R' = 4-MeO, R" = H
8c R = 4-Me, R' = 4-MeO, R" = 4-Cl
8d R = 4-Me, R' = 4-MeO, R" = 4-Me
8e R = 4-Me, R' = 4-MeO, R" = 3,4-diMeO
8f R = 4-MeO, R' = 4-MeO, R" = H
8g R = 4-MeO, R' = 4-MeO, R" = 4-Cl
8h R = 4-MeO, R' = 4-MeO, R" = 4-Me
8i R = 4-MeO, R' = 4-MeO, R" = 4-MeO
8j R = 4-MeO, R' = 4-MeO, R" = 3,4-diMeO
8l R = 3,4-diMeO, R' = 4-Et, R" = H
8m R = 3,4-diMeO, R' = 4-Et R" = 4-Cl
8n R = 3,4-diMeO, R' = 4-Et, R" = 4-Me
8o R = 3,4-diMeO, R' = 4-Et R" = 4-MeO

8k R = 4-MeO, R' = 4-MeO
8p R = 3,4-diMeO, R = 4-Et

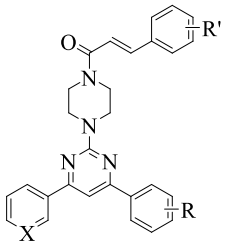

8q R = 4-Cl, R =Me

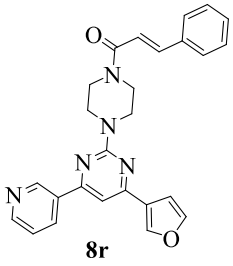

8r

Fig. 4. The structures of the pyrimidine-cinnamoyl derivatives (**8a-r**).

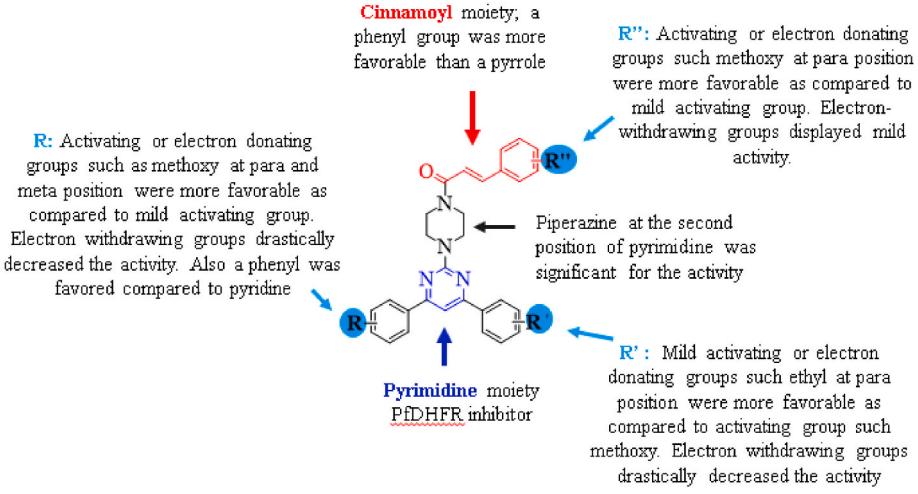

Fig. 5. Structure-Activity Relationship (SAR) of cinnamoyl-pyrimidine compounds.

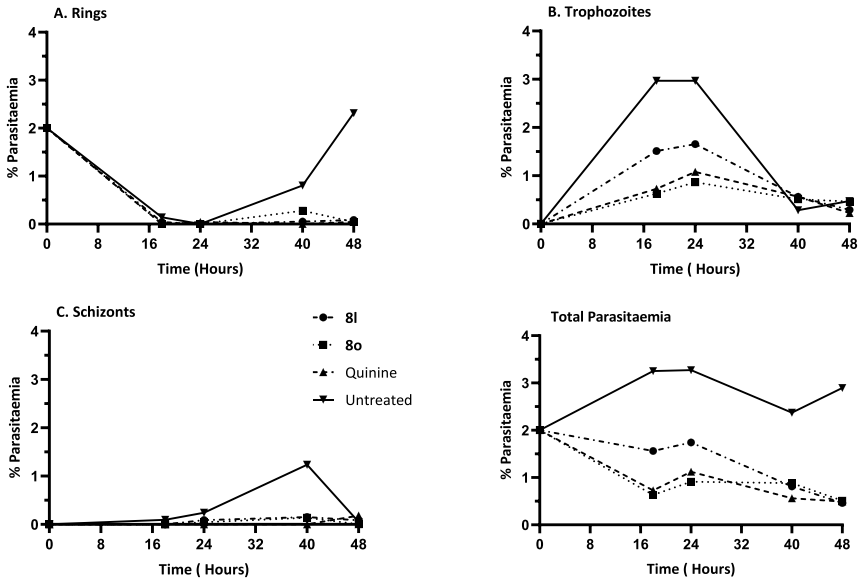

Fig. 6. Stage-dependent activity of **8l** and **8o** over a 48 h period of the ring (**A**), trophozoite (**B**), schizont (**C**) stages and the total % parasitaemia (**D**) following exposure to the 50 % inhibitory concentrations of the respective analogues compared to untreated and quinine-treated parasites.

7. Conformational stability and flexibility of Apo and protein-bound systems

To further investigate the structural and conformational changes that might impact the biological activity of the two proteins, the parameters RMSD, RoG, RMSF, and SASA of alpha carbon (Cα) atoms for the unbound (Apo) and bound systems were performed. The structural analysis of the parameters was monitored throughout 100 ns M.D. simulations and plotted to understand the dynamics of the two protein systems. The root mean square deviation (RMSD) measures the System's convergence, the drift of the unbound structure, and the structural stability [39]. For the PfHsp70-1 system, all four compounds achieved convergence in less than 8 ns M.D. simulation, compared to the unbound systems, which achieved convergence in approximately 10 ns M.D. simulation. Signifying the bound systems reached structural stability and maintained stable conformation earlier than the unbound enzyme. Fig. 10 shows the graphical representation of the systems' alpha carbon (Cα) atoms RMSD. From the result of the plot, it could be inferred that compounds **8l** and **8o** have the highest RMSD values, followed by **8m**, **8k**, and **Apo**. The alpha carbon (Cα) atom RMSD backbone atoms of all arrangements were relatively stable. However, the RMSD of the Apo (4.0 A) was lower than the RMSD of the bound system, which converged (RMSD 8.0 A) for **8k**, **8m** and **8o**, while in the case of **8l,** it converged to RMSD 12Å. The average RMSDs (Å) of Apo, **8m**, **8o**, **8k,** and **8l** were 7.78, 9.14, 10.38, 11.38, and 11.79, respectively, and the order of increasing stability follows Apo < **8m** < **8o** < **8k** < **8l**. Compared with the unbound Apo system, the high stability of the bound system could be due to the inward-pulling interactions of the residues with the bound system [50]. Similarly, for PfHsp70-z system, all four compounds converged at around 20 ns M.D. simulation to the unbound system. They all converged around RMSD 8.0Å. The average RMSDs (Å) of **8m**, **8k**, **8l**, **8o**, and Apo were 8.18, 8.42, 9.38, 9.62, and 9.66, respectively, and the order of increasing stability follows Apo >**8m** >, **8o** > **8k** > **8l**. In the case of the PfHsp70-1 system, the average RMSD shows that the compound's RMSD values are higher, as displayed in the diagram in Fig. 10, than that of the Apo. While in the case of the PfHsp70-z system, the average RMSD for each compound is lower than the Apo. This suggests that the deviations achieved in both cases point to the influence of the compounds on the proteins, which eventually resulted in their stability.

The root mean square fluctuation RMSF of the complexes **8m**, **8k**, **8l**, **8o,** and unbound systems were studied to examine the flexibility and stability of individual amino residues of the proteins. The RMSF monitors the ligand's binding effect on the vibration of the individual active residues of a protein [40]. The higher and lower fluctuation values indicated more and less flexible movements. As displayed in Fig. 4, residues 200–300, 400–500, and 502–548 fluctuate in all four compounds and the unbound PfHsp70-1 system. While most of the residues around (150–250) and (300–399) involved in ligand binding fluctuate less. The plot further revealed that the average RMSF values of the compounds **8m** (8.940 Å) and **8o** (10.341 Å) were higher fluctuations than the unbound System with an average RMSF value of 8.725 Å. While compounds **8k** and **8l** exhibited less fluctuation than the unbound enzyme, with average values of 6.607 Å and 7.729 Å, respectively. In the case of the PfHsp70-z systems, **8l**, **8o**, and **8k** exhibited lower fluctuation of 7.965 Å, 8.346 Å, and 9.631 Å than the unbound System with an average RMSF value of 9.710 Å. But compound **8m** showcased a higher average fluctuation of 10.238 Å.

The shape and folding of the unbound and bound-protein systems could further be explored by measuring the radius of distribution/gyration (RoG) around the residue C-atoms from the centre of mass. Therefore, this analysis provides the compactness of a protein that undergoes some dynamic forces. High RoG values depict a less tight structure and increased mobility. The radius of gyration of C-atoms of PfHsp70-1 system measured before and after binding **8k, 8l, 8m,** and **8o** in separate unbound Systems over 100 ns. The average RoG (Å) of bound systems is **8o** (33.267 Å), **8k** (31.837 Å) and **8m** (31.143 Å) and **8l** (26.328 Å), respectively, and the unbound system PfHsp70-1 (30.062 Å). This implies the compounds did not show similar compactness. It also shows that complex **8o, 8k,** and **8m** have higher average RoG than the unbound complex suggesting low stability, while complex **8l** shows a lower average RoG than the unbound system indicating high stability. Unlike for the PfHsp70-z System, the average RoG for **8k, 8l, 8o,** and **8m** are 34.193 Å, 34.494 Å, 33.084 Å and 31.287 Å, whereas the unbound is 29.815 Å indicating low stability for the PfHsp70-z systems.

Solvent-accessible surface area (SASA) investigates the effect of the binding of the ligand to a protein, and it quantifies the enzyme exposure to solvent molecules [41]. The four compounds, **8m, 8k, 8o,** and **8l,** exhibited an increase in the exposure of the enzyme to solvent molecules, as their respective bindings raised the average SASA values when compared to the unbound PfHsp70-1 (Fig. 10). SASA mean values of

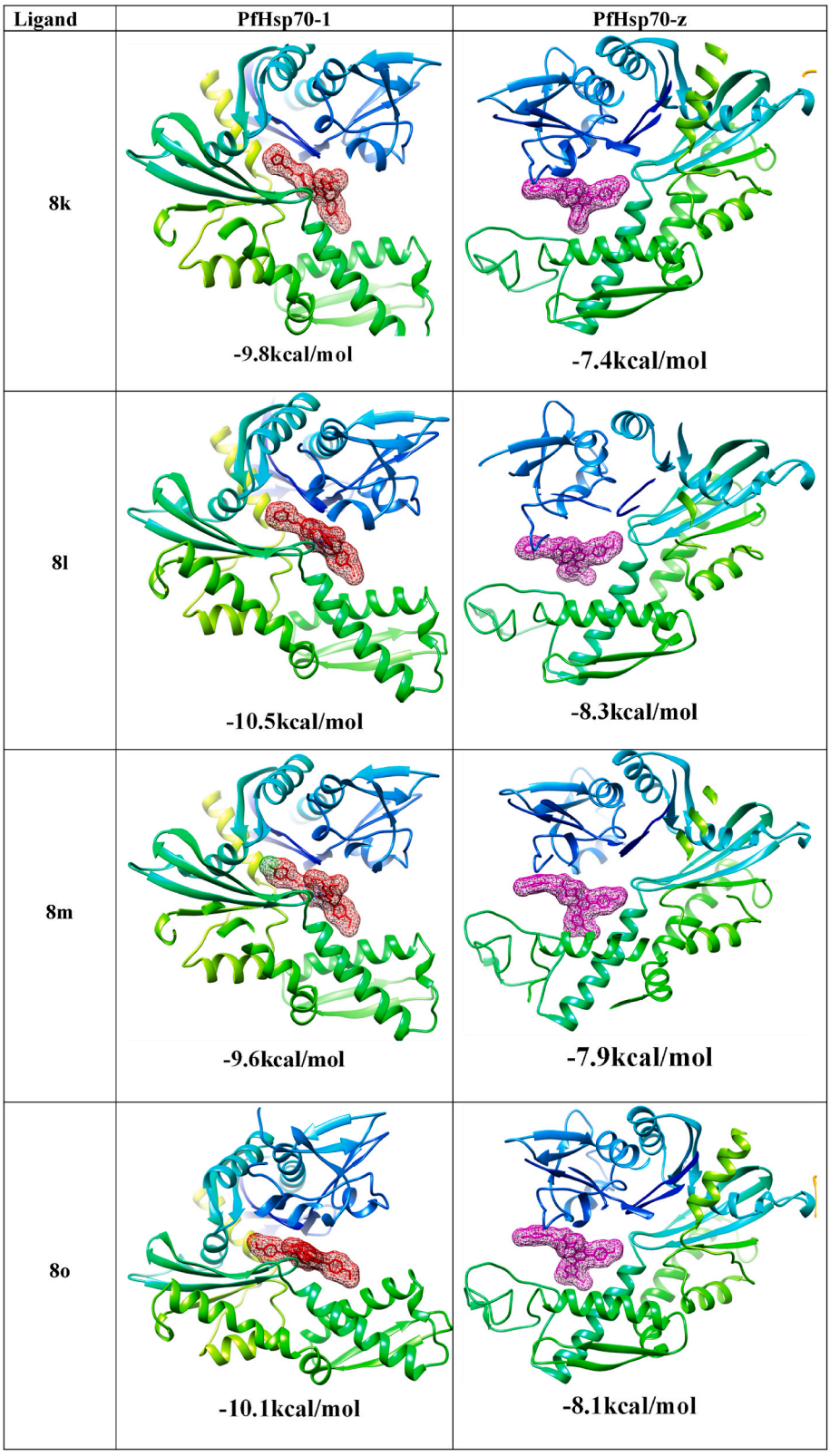

Fig. 7. Docking scores and Binding modes of the compounds to PfHsp70-1 and PfHsp70-z.

26996 Å^2, 26926 Å^2, 26468 Å^2, 25465 Å^2 and 26.506 Å^2 were recorded for compounds **8m, 8k, 8o, 8l** and unbound PfHsp70-1. The average SASA values for compounds **8m, 8o, 8k, 8l,** and the unbound PfHsp70-z systems are 35437 Å^2, 35175 Å^2, 34836 Å^2, 34441 Å^2, and 34491 Å^2 respectively (Fig. 11). The increased SASA values reported for the compounds showed the binding of the compounds further exposed the enzyme to a solvent molecule. This suggests that the structural integrity of the enzyme was not distorted after 100 ns.

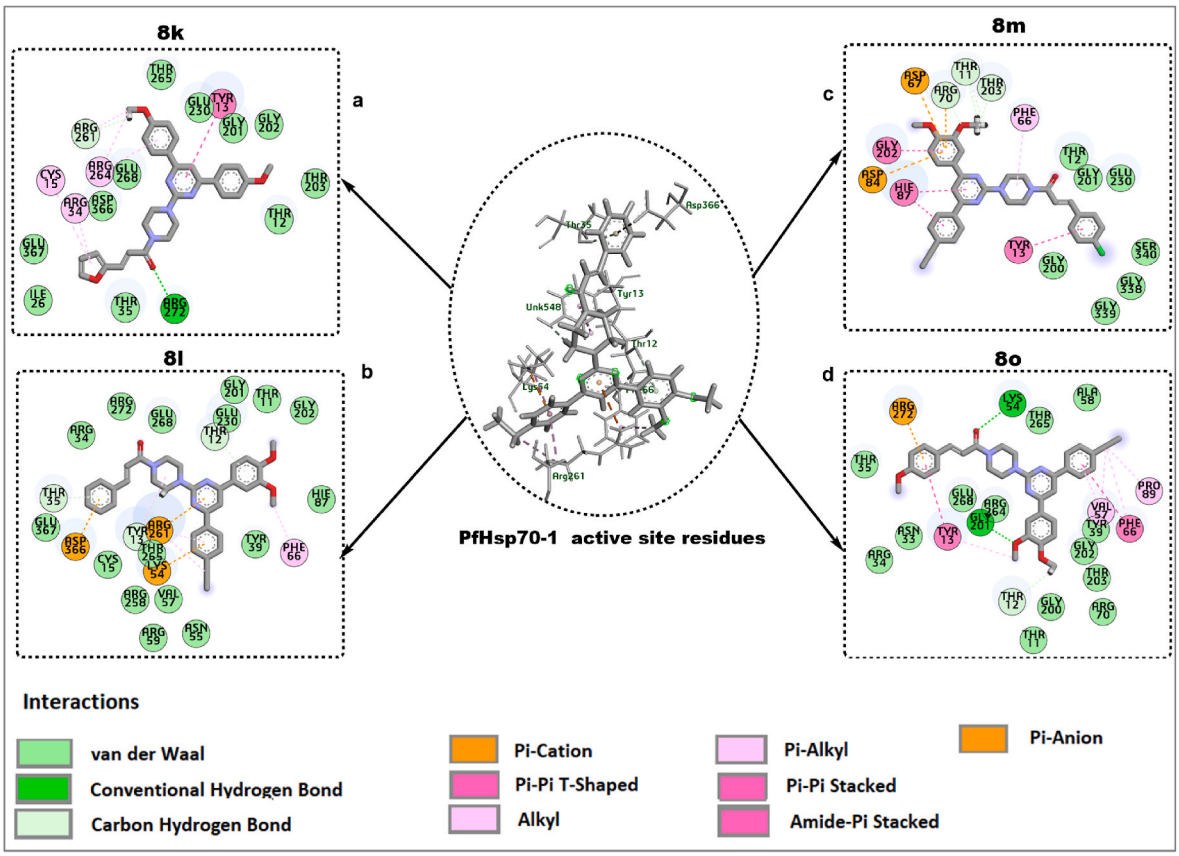

Fig. 8. Interaction types and receptor (PfHsp70-1)-ligand interactions plots of (a) **8k**, (b) **8l**, (c) **8m**, and (d) **8o.**

8. Accessing the ADME and drug-likeness of the compounds

Physiochemical and pharmacokinetic properties of the four compounds were predicted, as displayed in Table 4, using the SwiswADME application [42]. For a potential drug, its physical and chemical properties must adhere to the Lipinski rule of 5 to ascertain its safety as an oral drug [43]. The four compounds (**8k, 8l, 8m, and 8o**) had zero hydrogen bond donors and not more than 10 hydrogen bond acceptors. However, only **8k, 8l, 8m** and **8o** passed the drug-likeness test, with **8l, 8m** and **8o** showing a single violation (M.Wt. > 500), with one violation (M.Wt. > 500). However, compared to the standard drug Chloroquine **(CQ)**, only compound **8k** displayed no violation. Moreover, the partition coefficients (log P) were around 5. Compound **8o** failed the test because it violated 2 out of 5 Lipinski's rules. Moreover, the partition coefficients (log P) of the compounds were around 5. Usually, a larger LogP value indicates a low probability that the drug will permeate the lipid membrane. However, only **8k** and **8m** demonstrated low LogP of less than 5, similar to **CQ**. All four compounds (**8k, 8l, 8m, and 8o**) were predicted to have high absorption from the GIT. This suggests that all four compounds would attain optimal concentrations in the systemic circulation, as shown by the standard drug [44].

The blood-brain barrier (BBB) is a protective gate that prevents the passage of toxic compounds into the brain or the central nervous system. None of the four compounds were predicted to permeate through the BBB. The number of hydrogen donors was zero for the four test compounds (**8k, 8l, 8m,** and **8o**), while the hydrogen acceptors were 6–9. Thus, indicating that all test compounds could be considered orally active. Drug bioavailability measures the degree of absorption and the fraction of a given amount of unchanged drug that goes to the systemic circulation [42]. Compounds **8k, 8l,** and **8m** showed a relatively high score of 0.55 except compound **8o**, with a score of 0.17, suggesting that only the first three compounds might reach their active sites with higher concentrations required for therapeutic effect.

9. Conclusion

In summary, we present a library of novel pyrimidine-cinnamoyl hybrids merged by piperazine and their associated antiplasmodial activities and pharmacokinetic properties, along with proposed mechanism of action. The ready-to-use chemical reagents, reactants, and excellent yields (80–90 %) make this synthetic strategy enticing and methodical. Specifically, compounds **8l** and **8o** displayed the most promising leads exhibiting excellent antimalarial activity against *P. falciparum* with a selective index of 16.75 and 18.59, respectively. The findings of this study propose how beneficial it is to incorporate a piperazine linker to amalgamate the fragments of pyrimidine and cinnamoyl moiety and the designed compounds, thus laying a good foundation for further lead optimization. Interestingly, both compounds demonstrated significant affinity towards the two essential molecular chaperones of *P. falciparum*. It should be noted that only compound **8k** is considered a more preferred ligand compared to **8l**, **8m** and **8o** because it passed the Lipinski's rule of five for drug-likeness properties. Future studies could improve the antimalarial activity of the compounds by varying the phenyl substituents and through comprehensive supplemental functionalism, which promises an investigation.

10. Chemistry section

All chemical reagents utilized in this research were acquired from Sigma-Aldrich and Merck Millipore, South Africa. The commercially accessible chemicals Benzaldehyde and acetophenone were obtained from Sigma- Aldrich (South Africa). All solvents, except those of laboratory reagent grade, were dried and purified when required as per formerly published procedures. The progression of the chemical

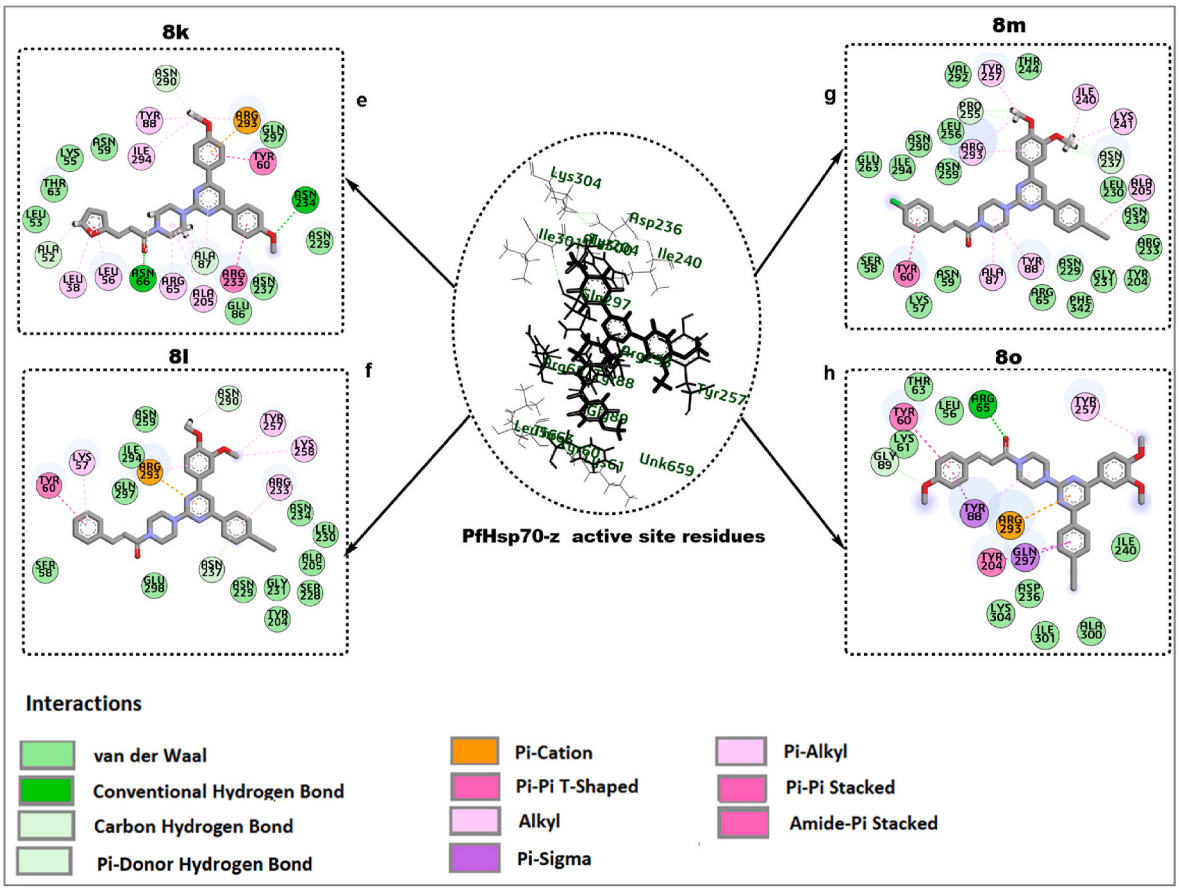

Fig. 9. Interaction types and receptor (PfHsp70-z)-ligand interaction plots of (e) **8k**, (f) **8l**, (g) **8m**, and (h) **8o.**

reactions and the purity of the compounds was monitored by thin-layer chromatography (TLC) on precoated silica gel plates secured with E. Merck and Co. (Darmstadt, Germany) using 36 % ethyl acetate in n-hexane as the mobile phase and iodine vapour as the visualizing agent.

The melting points of the synthesized compounds were resolved by a Thermo Fisher Scientific (IA9000, U.K.) digital melting point apparatus and are uncorrected. The IR spectra were recorded on a Bruker Alpha FT-IR spectrometer (Billerica, MA, USA) using the ATR technique. The ^{1}H NMR and ^{13}C NMR spectra were recorded on Bruker AVANCE 400 and 600 MHz (Bruker, Rheinstetten/Karlsruhe, Germany) spectrometers using $CDCl_3$ and DMSO-d_6. The chemical shifts are reported in δ ppm units using TMS as an internal standard. HRMS spectra were recorded on an Autospec mass spectrometer with electron impact at 70 eV.

10.1. A typical procedure for the synthesis of (E) chalcone

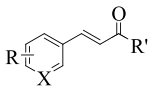

1a	X = H,	R = 4-Cl,	R' = 4-methoxyphenyl
1b	X = H,	R = 4-Me,	R' = 4-methoxyphenyl
1c	X = H,	R = 4-MeO,	R' = 4-methoxyphenyl
1d	X = H,	R = 3,4-MeO,	R' = 4-ethylphenyl
1e	X = N,	R = 4-H,	R' = 4-chlorophenyl
1f	X = N,	R = 4-H,	R' = furan-2-yl

To a stirred solution of acetophenone (5 gm, 32.34 mmol) in EtOH (30 ml) was added 60 % NaOH solution (12 gm NaOH/H_2O (20 mL)). The reaction was stirred at room temperature for 30 min, after which benzaldehyde (4.7 gm, 38.81 mmol) was added, and the reaction mixture was sonicated for 1 h at 35°C. The development of the product was monitored by TLC. Excess ethanol was removed under vacuum, and the reaction mixture was added to 100 gm of ice and stirred. The precipitates formed were filtered, washed with extra water, and dried. The crude product was purified by recrystallisation in EtOH to obtain the following pure compounds.

(E)-3-(4-chlorophenyl)-1-(4-methoxyphenyl) prop-2-en-1-one (**1a**): Yellow solid, yield: 96 %, mp = 130–133 °C; ^{1}H NMR (400 MHz, $CDCl_3$, δ, ppm): 8.03 (d, J = 8.85 Hz, 2H, ArH), 7.74 (d, J = 15.65 Hz, 1H, Ph-C**H**=CH), 7.57 (d, J = 8.49 Hz, 2H, ArH), 7.51 (d, J = 15.63 Hz, 1H, Ph-CH=C**H**), 7.38 (d, J = 8.49, Hz, 2H ArH), 6.98 (d, J = 8.84, Hz, 2H ArH), 3.89 (s, 3H, OCH_3); ^{13}C NMR (100 MHz, $CDCl_3$, δ ppm): 188.40, 163.55, 142.47, 136.18, 136.18, 133.58, 130.91, 122.27, 113.91, 55.53 (OCH_3); HRMS (ESI, *m/z*) $[M+H]^+$; calculated for $C_{16}H_{13}ClO_2$, 273.0682.

(E)-1-(4-methoxyphenyl)-3-(p-tolyl)prop-2-en-1-one (**1b**): Yellow Solid. yield: 98 %, mp = 125–128 °C; ^{1}H NMR (400 MHz, $CDCl_3$, δ, ppm): 8.04 (d, J = 8.76 Hz, 2H, ArH), 7.89 (d, J = 15.60 Hz, 1H, Ph-C**H**=CH), 7.54 (d, J = 7.95 Hz, 2H, ArH), 7.51 (d, J = 15.63 Hz, 1H, Ph-CH=C**H**), 7.22 (d, J = 7.97, Hz, 2H ArH), 6.98 (d, J = 8.77 Hz, 2H, ArH), 3.88 (s, 3H, CH_3), 2.39 (s, 3H,CH_3); ^{13}C NMR (100 MHz, $CDCl_3$, δ ppm): 189.43 (C=O), 163.92, 144.64, 1410.40, 132.92, 131.81, 131.34, 130.24, 128.96, 121.46, 114.39, 56.06(OCH_3), 22.09 (CH_3); HRMS (ESI, *m/z*) $[M+H]^+$; calculated for $C_{17}H_{16}O_2$, 253.1228.

(E)-1,3-bis(4-methoxyphenyl)prop-2-en-1-one (**1c**): Yellow solid, yield: 86 %, mp = 102–104 °C; ^{1}H NMR (400 MHz, $CDCl_3$, δ, ppm): 8.03 (d, J = 8.75 Hz, 2H, ArH), 7.78 (d, J = 15.58 Hz, 1H, Ph-C**H**=CH), 7.60 (d, J = 8.66 Hz, 2H, ArH) 7.43 (d, J = 15.58 Hz, 1H, Ph-CH=C**H**), 6.96 (dd, J = 17.58, 8.72 Hz, 4H, ArH), 3.89 (s, 3H, OCH_3), 3.85 (s, 3H, OCH_3); ^{13}C NMR (100 MHz, $CDCl_3$, δ ppm): 189.39 (C=O), 163.84, 162.09, 162.09, 144.39, 131.95, 131.28, 130.67, 128.40, 120.15,

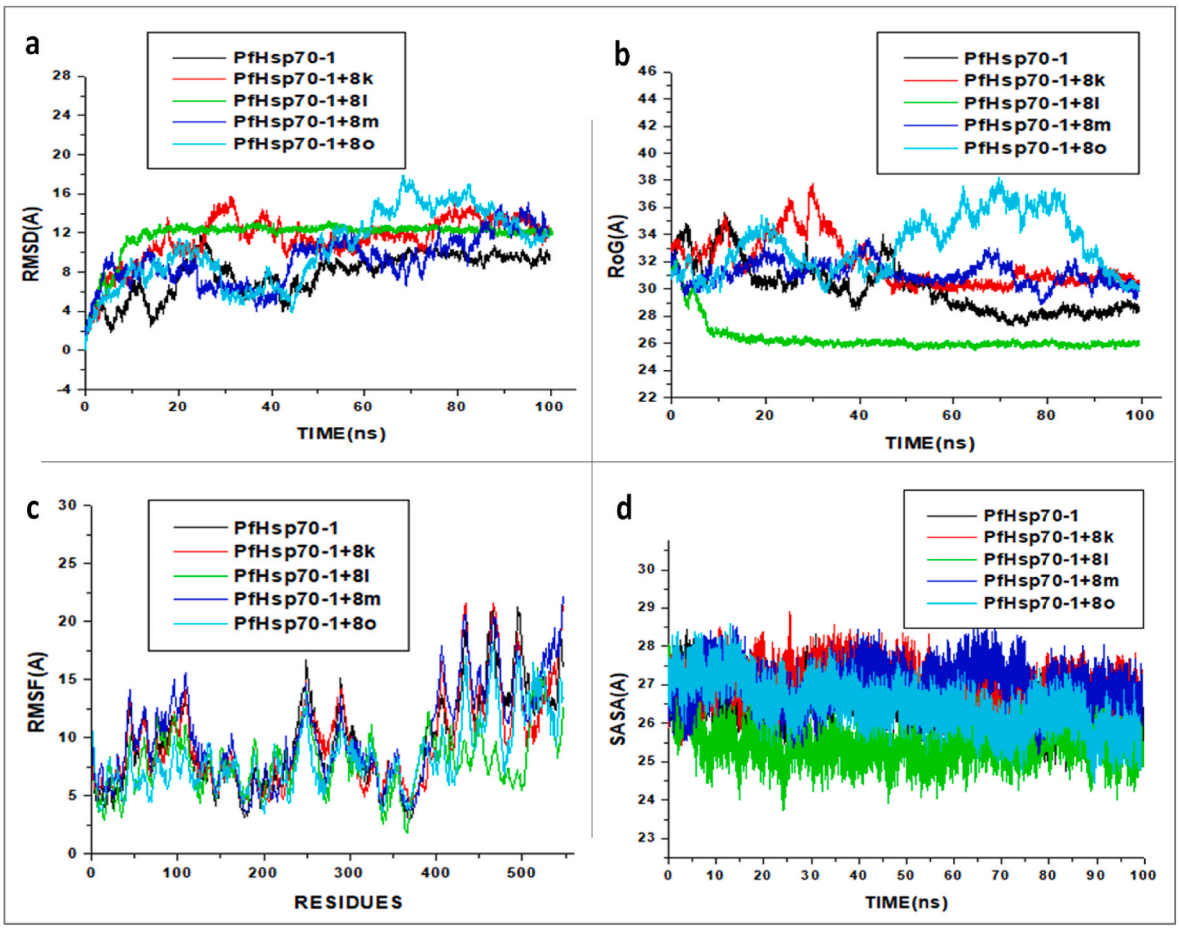

Fig. 10. Plots of alpha C atoms of the PfHsp70-1, **8k**, **8l**, **8m**, and **8o**, a) RMSD plot, b) RoG c) RMSF, and d) SASA plot systems calculated throughout 100 ns M.D. simulations.

114.96, 114.36, 56.05 (OCH_3), 55.98 (OCH_3); HRMS (ESI, *m/z*) $[M+H]^+$; calculated for $C_{17}H_{16}O_3$, 269.1177.

(E)-3-(3,4-dimethoxyphenyl)-1-(4-methoxyphenyl)prop-2-en-1-one (**1f**): Yellow solid, yield: 81 %, mp = 80–83 °C; ^{1}H NMR (400 MHz, $CDCl_3$, δ, ppm): 8.03 (d, J = 8.81 Hz, 2H, ArH), 7.75 (d, J = 15.56 Hz, 1H, Ph-C**H**=CH), 7.40 (d, J = 15.56 Hz, 1H, Ph-CH=C**H**), 7.23 (dd, J = 8.31, 1.64 Hz, 1H, ArH), 7.16 (s, 1H, ArH), 6.98 (d, J = 8.81 Hz, 1H, ArH), 6.89 (d, J = 8.27 Hz, 1H, ArH), 3.94 (s, 3H, OCH_3), 3.92 (s, 3H, OCH_3), 3.88 (s, 3H, OCH_3); ^{13}C NMR (100 MHz, $CDCl_3$, δ ppm): 189.37 (C=O), 163.86, 151.83, 149.80, 144.71, 131.89, 131.29, 128.65, 123.53, 120.42, 114.36, 111.70, 110.68, 56.56 (OCH_3), 56.54 (OCH_3), 56.05 (OCH_3); HRMS (ESI, *m/z*) $[M+H]^+$; calculated for $C_{18}H_{18}O_4$, 299.1283.

10.2. Typical procedure for the synthesis of 4,6-diphenylpyrimidin-2-amine

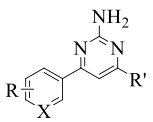

2a	X = H,	R = 4-Cl,	R' = 4-methoxyphenyl
2b	X = H,	R = 4-Me,	R' = 4-methoxyphenyl
2c	X = H,	R = 4-MeO,	R' = 4-methoxyphenyl
2d	X = H,	R = 3,4-MeO,	R' = 4-ethylphenyl
2e	X = N,	R = 4-H,	R' = 4-chlorophenyl
2f	X = N,	R = 4-H,	R' = furan-2-yl

The reaction mixture of (*E*) chalcone (8 gm, 31.16 mmol), Guandine. HCl (4.8 gm, 49.86 mmol), and 60 % NaOH (12 gm NaOH/H_2O (20 mL)) in EtOH (30 mL) were refluxed for 24 h. The development of the product was monitored using TLC. Excess ethanol was removed under vacuum using rotavapor. The reaction mixture was then added to 100 gm of ice water, and the precipitate formed was filtered, washed with excess water, and dried. The crude compound was purified by column chromatography using EtOAc/Hexane (1:4) eluent to obtain the following pure compounds.

4-(4-chlorophenyl)-6-(4-methoxyphenyl)pyrimidin-2-amine (**2a**): Yellow solid, yield: 58 %, mp = 127–129 °C; ^{1}H NMR (400 MHz, $CDCl_3$, δ, ppm): 8.03 (d, J = 8.78 Hz, 2H, ArH), 7.95 (d, J = 8.06 Hz, 2H, ArH), 7.39 (s, 1H, Pyr-H), 7.29 (d, J = 7.98 Hz, 2H, ArH), 7.00 (d, J = 8.76 Hz, 2H, ArH), 5.15 (s, 2H, NH_2), 3.88 (s, 3H, CH_3), 2.42 (s, 3H, CH_3); ^{13}C NMR (100 MHz, $CDCl_3$, δ ppm): 189.43, 163.92, 144.64, 141.40, 132.92, 131.34, 130.24, 128.96, 121.46, 114.39, 56.06 (OCH_3), 22.89 (CH_3).

4-(4-methoxyphenyl)-6-(p-tolyl)pyrimidin-2-amine (**2b**): Yellow solid, yield: 64 %, mp = 127–129 °C; ^{1}H NMR (400 MHz, $CDCl_3$, δ, ppm): 8.03 (d, J = 8.64 Hz, 2H, ArH), 8.00 (d, J = 8.36 Hz, 2h, ArH), 7.46 (d, J = 8.36 Hz, 2H, ArH), 7.37 (s, 1H, Pyr-H), 7.00 (d, J = 8.56 Hz, 2H, ArH) 5.20 (s, 2H, NH_2), 3.88 (s, 3H, CH_3); ^{13}C NMR (100 MHz, $CDCl_3$, δ ppm): 165.88, 164.64, 163.55, 161.76, 136.47, 136.47, 129.91, 128.96, 128.64, 128.40, 114.14, 103.18, 55.43 (OCH_3).

4,6-bis(4-methoxyphenyl) pyrimidin-2-amine (**2c**): Yellow solid, yield: 65 %, mp = 171–173 °C; ^{1}H NMR (400 MHz, $CDCl_3$, δ, ppm): 8.04 (d, J = 8.66 Hz, 4H, ArH), 7.36 (s, 1H, Pyr-H) 7.00 (d, J = 8.69 Hz,4H, ArH), 5.36 (s, 2H, NH_2), 3.87 (s, 6H, $2CH_3$); ^{13}C NMR (100 MHz, $CDCl_3$, δ ppm): 165.19, 162.97, 161.77, 129.78, 128.69, 114.15, 102.64, 55.43 (OCH_3).

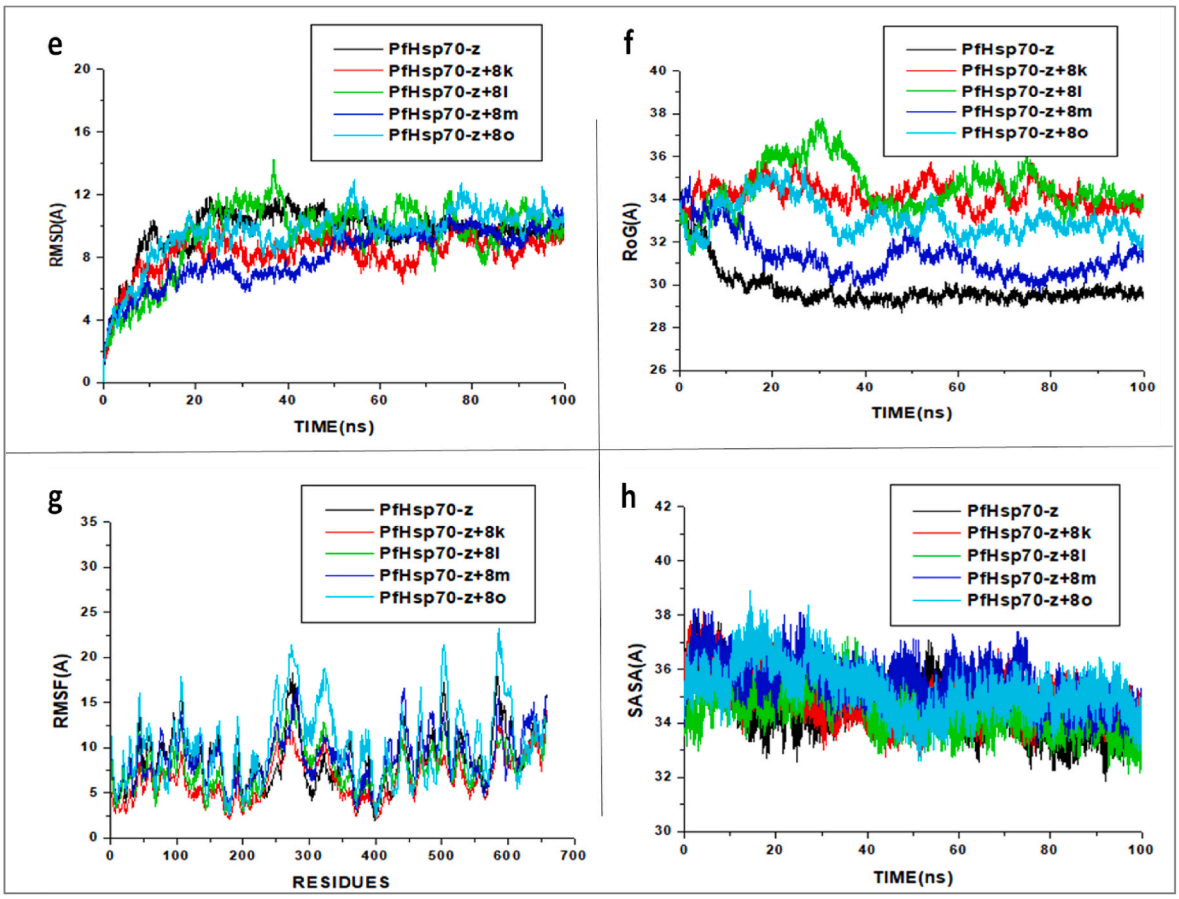

Fig. 11. Plots of alpha C atoms of the PfHsp70-z, **8k**, **8l**, **8m** and **8o**, e) RMSD plots, f) RoG g) RMSF and h) SASA plot systems calculated throughout 100 ns M.D. simulations.

Table 4
Physiochemical, Pharmacokinetic, and drug-likeness properties of the compounds.

Compd	M.Wt **g/mol**	H-bond donor	H-bond **Acceptor**	Lipophilicity (iLOGP)	Water Solubility	GIT Absorption	BBB Permeability	Bioavailability Score	Drug likeness (Lipinski)
8k	585.62	0	9	5.28	Poor	High	No	0.55	Yes (1)
8l	523.67	0	6	5.11	Poor	High	No	0.55	Yes (1)
8m	533.62	0	7	5.02	Poor	High	No	0.55	Yes (1)
8o	578.62	0	9	4.76	Poor	High	No	0.17	No (2)
CQ	319.87	1	2	3.95	poor	High	Yes	0.55	Yes (0)

4-(3,4-dimethoxyphenyl)-6-(4-ethylphenyl)pyrimidin-2-amine (**2d**): Yellow solid, yield: 61 %; ^{1}H NMR (400 MHz, $CDCl_3$, δ, ppm): 8.26 (d, J = 8.23 Hz, 2H, ArH), 7.97 (dd, J = 7.98 Hz,1.94 Hz, 1H, ArH), 7.89 (s, 1H, Pyr-H), 7.88 (d, J = 8.20 Hz, 1H, ArH), 7.38 (d, J = 8.26 Hz, 2H, ArH), 7.10 (d, J = 8.59 Hz, 1H, ArH), 3.92 (s, 3H, OCH_3), 3.86 (s, 3H, OCH_3), 2.70 (q, J = 5.68 Hz, 2H, $2CH_2$), 1.23 (t, J = 7.58 Hz, 3H CH_3); ^{13}C NMR (100 MHz, $CDCl_3$, δ ppm): 165.07, 164.63, 162.12, 151.08, 149.11, 146.83, 135.80, 131.15, 128.18, 127.11, 120.94, 110.10, 101.30, 56.04 (OCH_3), 56.02 (OCH_3), 28.81 (CH_2), 15.52 (CH_3).

4-(furan-2-yl)-6-(pyridin-3-yl)pyrimidin-2-amine (**2f**): Yellow solid, yield: 65 %; ^{1}H NMR (400 MHz, DMSO-d_6, δ, ppm): 8.36 (s, 1H, ArH) 8.75 (d, J = 3.92 Hz, 1H, ArH), 8.52 (d, J = 8.00 Hz, 1H, ArH), 8.24 (d, J = 8.52 Hz, 2H, ArH), 7.82 (s, 1H, Pyr-H), 7.63 (d, J = 8.60 Hz, 2H, ArH), 7.59 (dd, J = 7.96 Hz, 4.80 Hz, 1H, ArH); ^{13}C NMR (100 MHz, DMSO-d_6, δ ppm): 151.93, 148.61, 136.43, 135.02, 129.41, 128.91, 123.78.

10.2.1. A typical procedure for the synthesis of 4,6-diphenylpyrimidin-2-ol (3a-f)

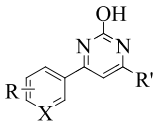

3a	X = H,	R = 4-Cl,	R' = 4-methoxyphenyl
3b	X = H,	R = 4-Me,	R' = 4-methoxyphenyl
3c	X = H,	R = 4-MeO,	R' = 4-methoxyphenyl
3d	X = H,	R = 3,4-MeO,	R' = 4-ethylphenyl
3e	X = N,	R = 4-H,	R' = 4-chlorophenyl
3f	X = N,	R = 4-H,	R' = furan-2-yl

To the stirring solution of 4,6-diphenylpyrimidin-2-amine **2** (4 gm, 12.76 mmol) in acetic acid (50 mL) was slowly added a solution of 10 eq.

$NaNO_2$ in H_2O (50 mL) at room temperature. The reaction mixture was further stirred for 3 h. The development of the product was monitored using TLC. The precipitate formed was filtered, washed with excess water, and dried. The crude product was recrystallized from EtOH to obtain the following pure compounds.

4-(4-chlorophenyl)-6-(4-methoxyphenyl)pyrimidin-2-ol (**3a**): Yellow solid, yield: 83 %, mp = 235–237 °C; ^{1}H NMR (400 MHz, DMSO-d_6, δ, ppm): 11.94 (s, 1H, Pyr-O**H**), 8.18 (dd, J = 18.36 Hz, 8.53Hz, 4H, ArH), 7.62 (d, J = 8.60 Hz, 2H, ArH), 7.56 (s, 1H, Pyr-H), 7.10 (d, J = 8.89 Hz, 2H, ArH), 3.85 (s, 3H, OCH_3); ^{13}C NMR (100 MHz, DMSO-d_6, δ ppm): 162.11, 136.20, 129.37, 128.81, 127.49, 114.23, 55.48 (OCH_3).

4-(4-methoxyphenyl)-6-(p-tolyl)pyrimidin-2-ol (**3b**): Yellow solid, yield: 88 %, mp = 235–237 °C; ^{1}H NMR (400 MHz, DMSO-d_6, δ, ppm): 11.85 (s, 1H, Pyr-O**H**), 8.16 (d, J = 8.74 Hz, 2H, ArH), 8.04 (d, J = 7.97 Hz, 2H, ArH), 7.44 (s, 1H, Pyr-H), 7.35 (d, J = 7.98 Hz, 2H, ArH), 7.09 (d, J = 8.97 Hz, 2H, ArH), 3.85 (s, 3H, OCH_3), 2.39 (s, 3H, CH_3); ^{13}C NMR (100 MHz, DMSO-d_6, δ ppm): 162.05, 141.51, 129.39, 129.35, 127.46, 114.18, 55.46 (OCH_3), 55.99 (CH_3).

4,6-bis(4-methoxyphenyl)pyrimidin-2-ol (**3c**): Yellow solid, yield: 79 %, mp °C; ^{1}H NMR (400 MHz, DMSO-d_6, δ, ppm): 11.82 (s, 1H, Pyr-O**H**), 8.14 (d, J = 8.53 Hz, 2H, ArH), 7.41 (s, 1H, Pyr-H), 7.09 (d, J = 8.91 Hz, 2H, ArH), 3.85 (s, 6H, $2OCH_3$); ^{13}C NMR (100 MHz, DMSO-d_6, δ ppm): 162.00, 129.32, 114.18, 55.46 ($2OCH_3$).

4-(3,4-dimethoxyphenyl)-6-(4-ethylphenyl)pyrimidin-2-ol (**3d**): Yellow solid, yield: 93 %; ^{1}H NMR (400 MHz, DMSO-d_6, δ, ppm): 12.02 (s, 1H, Pyr-O**H**), 8.26 (d, J = 8.23 Hz, 2H, ArH), 7.97 (dd, J = 7.98 Hz,1.94 Hz, 1H, ArH), 7.89 (s, 1H, Pyr-H), 7.88 (d, J = 8.20 Hz, 1H, ArH), 7.38 (d, J = 8.26 Hz, 2H, ArH), 7.10 (d, J = 8.59 Hz, 1H, ArH), 3.92 (s, 3H, OCH_3), 3.86 (s, 3H, OCH_3), 2.70 (q, J = 5.68 Hz, 2H, $2CH_2$), 1.23 (t, J = 7.58 Hz, 3H CH_3); ^{13}C NMR (100 MHz, DMSO-d_6, δ ppm): 165.07, 164.63, 162.12, 151.08, 149.11, 146.83, 135.80, 131.15, 128.18, 127.11, 120.94, 110.10, 101.30, 56.04 (OCH_3), 56.02 (OCH_3), 28.81 (CH_2), 15.52 (CH_3).

4-(furan-2-yl)-6-(pyridin-3-yl)pyrimidin-2-ol (**3f**): Yellow solid, yield: 90 %, mp °C; ^{1}H NMR (400 MHz, DMSO-d_6, δ, ppm), 12.21 (s, 1H, Pyr-O**H**), 9.36 (s, 1H, ArH) 8.75 (d, J = 3.92 Hz, 1H, ArH), 8.52 (d, J = 8.00 Hz, 1H, ArH), 8.24 (d, J = 8.52 Hz, 2H, ArH), 7.82 (s, 1H, Pyr-H), 7.63 (d, J = 8.60 Hz, 2H, ArH), 7.59 (dd, J = 7.96 Hz, 4.80 Hz, 1H, ArH); ^{13}C NMR (100 MHz, DMSO-d_6, δ ppm): 151.93, 148.61, 136.43, 135.02, 129.41, 128.91, 123.78.

10.3. A typical procedure for the synthesis of 2-chloro-4,6-diphenylpyrimidine

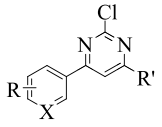

4a	X = H,	R = 4-Cl,	R' = 4-methoxyphenyl
4b	X = H,	R = 4-Me,	R' = 4-methoxyphenyl
4c	X = H,	R = 4-MeO,	R' = 4-methoxyphenyl
4d	X = H,	R = 3,4-MeO,	R' = 4-ethylphenyl
4e	X = N,	R = 4-H,	R' = 4-chlorophenyl
4f	X = N,	R = 4-H,	R' = furan-2-yl

A solution of 4,6-diphenylpyrimidin-2-ol (4 gm, 16.11 mmol) in $POCl_3$ (20 mL) catalytic amount of DMF (0.4 mL) was added and the reaction mixture was refluxed for 6 h. The development of the product was monitored using TLC. The reaction mixture was poured into crushed ice, and the precipitate formed was filtered, washed with water, and dried. The crude compound was purified by column chromatography using EtOAc/Hexane (1:9) eluent to obtain the following pure compounds.

2-chloro-4-(4-chlorophenyl)-6-(p-tolyl)pyrimidine (**4b**): Yellow solid, yield: 88 %; ^{1}H NMR (400 MHz, $CDCl_3$, δ, ppm): 8.09 (d, J = 8.52 Hz, 2H, ArH), 8.04 (d, J = 8.16 Hz, 2H, ArH), 7.94 (s, 1H, Pyr-H), 7.50 (d, J = 8.52 Hz, 2H, ArH), 7.33 (d, J = 8.00 Hz, 2H, ArH), 2.44 (s, 3H, CH_3); ^{13}C NMR (100 MHz, $CDCl_3$, δ ppm): 166.77, 165.13, 161.05, 141.46, 136.88, 133.16, 131.65, 128.83, 128.30, 127.68, 126.37, 109.20, 20.51 (CH_3).

2-chloro-4-(4-chlorophenyl)-6-(4-methoxyphenyl)pyrimidine (**4c**): Yellow solid, yield: 95 %; ^{1}H NMR (400 MHz, $CDCl_3$, δ, ppm): 8.11 (d, J = 8.84 Hz, 2H, ArH), 8.07 (d, J = 8.56 Hz, 2H, ArH), 7.88 (s, 1H, Pyr-H), 7.49 (d, J = 8.68 Hz, 2H, ArH), 7.02 (d, J = 8.92 Hz, 2H, ArH), 3.89 (s, 3H, OCH_3); ^{13}C NMR (100 MHz, $CDCl_3$, δ ppm): 167.27, 165.95, 162.75, 162.02, 137.82, 134.25, 129.30, 129.16, 128.67, 127.81, 114.46, 109.62, 55.50 (OCH_3).

2-chloro-4,6-bis(4-methoxyphenyl)pyrimidine (**4e**): Yellow solid, yield: 93 %, mp = 187–190 °C; ^{1}H NMR (400 MHz, $CDCl_3$, δ, ppm): 8.10 (d, J = 8.48 Hz, 3H, ArH), 7.87 (d, J = 8.84 Hz, 1H, ArH), 7.85 (s, 1H, Pyr-H), 7.01 (dd, J = 8.50 Hz, 1.74 Hz, 4H, ArH), 3.88 (s, 6H, $2OCH_3$); ^{13}C NMR (100 MHz, $CDCl_3$, δ ppm): 166.74, 166.52, 162.51, 161.84, 161.58, 131.61, 129.10, 128.19, 127.90, 114.39, 113.67, 109.01, 55.49 (OCH_3), 55.44 (OCH_3).

2-chloro-4-(3,4-dimethoxyphenyl)-6-(4-methoxyphenyl)pyrimidine (**4f**): Yellow solid, yield: 89 %, mp = 138–141 °C; ^{1}H NMR (400 MHz, $CDCl_3$, δ, ppm): 8.12 (d, J = 8.88 Hz, 2H, ArH), 7.87 (d, J = 8.84 Hz, 1H, ArH), 7.85 (s, 1H, Pyr-H), 7.01 (d, J = 8.88, 2H, ArH), 6.96 (d, J = 8.36, 1H, ArH), 4.00 (s, 3H, OCH_3), 3.95 (s, 3H, OCH_3), 3.88 (s, 3H, OCH_3); ^{13}C NMR (100 MHz, $CDCl_3$, δ ppm): 164.28, 164.24, 162.78, 161.40, 150.90, 149.06, 131.44, 131.04, 120.01, 113.92, 110.87, 110.05, 99.65, 56.00 (OCH_3), 55.95(OCH_3), 55.39(OCH_3).

2-chloro-4,6-bis(3,4-dimethoxyphenyl)pyrimidine (**4g**): Yellow solid, yield: 78 %, mp = 180–183 °C; ^{1}H NMR (400 MHz, $CDCl_3$, δ, ppm): 7.86 (s, 1H, ArH), 7.74 (s, 2H, ArH), 7.69 (d, J = 7.12 Hz, 2H, ArH), 6.97 (d, J = 7.76 Hz, 2H, ArH), 4.00 (s, 6H, $2OCH_3$), 3.96 (s, 6H, $2OCH_3$).

10.4. A typical procedure for the synthesis of 4,6-diphenyl-2-(piperazin-1-yl)pyrimidine (5a-d)

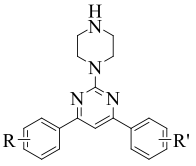

5a	R = 4-Cl	R' = 4- MeO
5b	R = 4-Me	R' = 4-MeO
5c	R = 4-MeO	R' = 4-MeO
5d	R = 3,4- MeO	R' = 4-Et

A reaction mixture of 2-chloro-4,6-diphenylpyrimidine **4** (4.0 g, 15 mmol) and piperazine (13.92 g, 150 mmol) in isopropanol (20 mL) was refluxed at 80 °C for 20 h. Using TLC, the progression of the reaction was monitored. The reaction mixture was added to 2 M NaOH (100 mL), the precipitate formed, and filtered, washed with water/diethyl ether, and dried under vacuum. The product was purified by recrystallized from EtOAc to afford the following pure compound(s).

4-(4-chlorophenyl)-6-(4-methoxyphenyl)-2-(piperazin-1-yl)pyrimidine (**5a**): Yellow solid, yield: 98 %; ^{1}H NMR (400 MHz, $CDCl_3$, δ, ppm): 8.25 (d, J = 8.76 Hz, 2H, ArH), 8.17 (d, J = 8.08 Hz, 1H, ArH), 7.70 (s, 1H, Pyr-H), 7.33 (d, J = 8.04 Hz, 2H, ArH), 3.93 (s.br, 4H, $2CH_2$), 3.84 (s, 3H, OCH_3), 2.57 (q, J = 4.42 Hz, 4H, $2CH_2$).

4-(4-methoxyphenyl)-2-(piperazin-1-yl)-6-(p-tolyl)pyrimidine (**5b**): Yellow solid, yield: 98 %; ^{1}H NMR (400 MHz, $CDCl_3$, δ, ppm): 8.26 (d, J = 8.79 Hz, 2H, ArH), 8.18 (d, J = 8.09 Hz, 2H, ArH), 7.70 (s, 2H, Pyr-H), 7.33 (d, J = 8.04 Hz, 2H, ArH), 7.07 (d, J = 8.79 Hz, 2H, ArH), 3.94 (s.

br, 4H, $2CH_2$) 3.85 (s, 3H, OCH_3), 2.58 (s.br, 4H, $2CH_2$), 2.38 (s, 3H, CH_3); ^{13}C NMR (100 MHz, DSMO-d_6, δ ppm): 164.90, 164.23, 164.09, 161.57, 161.50, 141.76, 140.55, 139.46, 134., 58, 132.46, 129.60, 129.47, 128.77, 128.29, 128.09, 127.05, 117.15, 114.11, 113.48, 100.68, 55.42 (OCH_3), 21.05, 21.03 (CH_3); HRMS (ESI, *m/z*) $[M+H]^+$; calculated for $C_{22}H_{24}N_4O$, 361.2028; Found 361.2067.

4,6-bis(4-methoxyphenyl)-2-(piperazin-1-yl*)pyrimidine* (**5c**): Brown solid, yield: 86 %, mp = 151–153 °C; FT-IR (ATR, ν_{max}, cm^{-1}): 3277 (N-H of N·H.), 2926-2845 (C-H of CH_3), 1172-1094 (C-N of pyr), 1256 (C-O of OCH_3), 1563 (C=N of pyr), 1605(C=C of Ar); ^1H NMR (400 MHz, DSMO-d_6, δ, ppm): 8.25 (d, J = 8.37 Hz, 4H, ArH), 7.67 (s, 1H, Pyr-H), 7.06 (d, J = 8.38 Hz, 4H ArH), 3.93 (s.br, 4H, $2CH_2$), 3.84 (s, 6H, $2OCH_3$), 3.37 (s, 2H, CH_2), 2.18 (s, 1H, C·H.), 2.60 (s.br, 4H, $2CH_2$); ^{13}C NMR (100 MHz, $CDCl_3$, δ ppm): ^{13}C NMR (400 MHz, DSMO-d_6, δ ppm): 163.70, 161.48, 161.28, 129.65, 128.58, 122.28, 113.92, 99.88, 55.28. ($2OCH_3$), 51.03 (CH_2), 46.11 ($2CH_2$), 43.26 ($2CH_2$).

4-(3,4-dimethoxyphenyl)-6-(4-ethylphenyl)-2-(piperazin-1-yl*)pyrimidine* (**5d**): Yellow solid, yield: 95 %, mp = 130–133 °C; ^1H NMR (400 MHz, $CDCl_3$, δ, ppm): 8.25 (d, J = 8.23 Hz, 2H, ArH), 7.96 (d, J = 7.98, 1.94 Hz, 1H, ArH), 7.88 (s, 1H, Pyr-H), 7.86 (d, J = 8.20 Hz, 2H, ArH), 7.28 (d, J = 8.26 Hz, 2H, ArH), 7.09 (d, J = 8.59 Hz, 1H, ArH), 4.33 (s. br, 4H, $2CH_2$) 3.91 (s, 3H, OCH_3), 3.85 (s, 3H, OCH_3), 3.76 (s.br, 4H, $2CH_2$), 2.70 (q, J = 7.57, 2H, CH_2), 1.23 (q, J = 7.58Hz, 3H, CH_3); ^{13}C NMR (100 MHz, DMSO-d_6, δ ppm): 164.38, 164.28,160.92, 151.37.148.83, 146.95, 134.44, 129.28, 128.08, 127.42, 127.28, 120.58, 111.48, 110.39, 101.95, 56.79, 55.79(OCH_3), 55.65 (OCH_3), 49.38 ($2CH_2$), 37.29 ($2CH_2$), 28.06 (CH_2), 15.46 (CH_3).

4-(furan-2-yl*)-2-(piperazin*-1-yl*)-6-(pyridin*-3-yl*)pyrimidine* (**5j**): Yellow solid, yield: 93 %; ^1H NMR (400 MHz, $CDCl_3$, δ, ppm): 8.75 (d, J = 3.94 Hz, 2H, ArH), 8.52 (d, J = 8.06 Hz, 1H, ArH), 8.24 (d, J = 8.55 Hz, 2H, ArH), 7.82 (s, 1H, Pyr-H), 7.63 (d, J = 8.61 Hz, 2H, ArH), 7.68 (d, J = 7.98 Hz, 1H, ArH), 3.93 (s.br, 4H, $2CH_2$), 2.56 (s.br, 4H, $2CH_2$).

10.5. A typical procedure for the synthesis of cinnamic acid

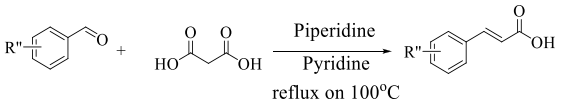

Benzaldehyde (2.0 g, 14.22 mmol), malonic acid (3.3g, 31.30 mmol), and piperidine (1.5 g, 17.07 mmol) in pyridine (30 mL) was refluxed for 24 h. The progression of the reaction was tracked by TLC. The crude was then added to 2 M HCl solution. The precipitate formed was filtered, washed with water, and dried to obtain the following pure compounds. No purification was needed.

(E)-3-(p-tolyl)acrylic acid (**6a**): yield: 98 %, Creamy white fluffy solid, mp = 195–198 °C; ^1H NMR (400 MHz, DMSO-d_6, δ, ppm): 12.31 (s, 1H, OH), 7.58–7.54 (m, 3H, ArH), 7.23 (d, J = 7.67 Hz, 2H, ArH), 6.46 (d, J = 16.01 Hz, 1H, Ph-CH=C**H**), 2.33 (s, 3H, CH_3); ^{13}C NMR (100 MHz, DMSO-d_6, δ ppm):144.38, 140.59, 140.43, 131.98, 129.97, 128.65, 118.57, 21.46;

(E)-3-(4-chlorophenyl)acrylic acid (**6b**): Creamy white fluffy solid, yield: 97 %, mp = 140–143 °C; ^1H NMR (400 MHz, DMSO-d_6, δ, ppm): 12.46 (s, 1H, O·H.), 7.72 (d, J = 8.51 Hz, 2H, ArH), 7.58 (d, J = 16.05 Hz, 1H, Ph-C**H**=CH), 7.46 (d, J = 8.48 Hz, 2H, ArH), 6.55 (d, J = 16.04 Hz, 1H, Ph-CH=C**H**); ^{13}C NMR (100 MHz, DMSO-d_6, δ ppm): 167.88, 142.97, 135.17, 133.74, 130.40, 129.39, 120.56.

(E)-3-(furan-2-yl*)acrylic acid* (**6c**):Yellow solid, yield: 89 %, mp = 142–144 °C; ^1H NMR (400 MHz, DMSO-d_6, δ, ppm): 12.40 (s, 1H), 7.83 (s, 1H), 7.38 (d, J = 16 Hz, 1H), 6.93 (d, J = 3.5 Hz, 1H), 6.62 ppm (t, J = 3.5 Hz, 1H), 6.15 (d, J = 16 Hz, 1H); ^{13}C NMR (100 MHz, DMSO-d_6, δ, ppm): 167.7, 150.7, 146.1, 131.2, 116.3, 115.9, 113.1.

10.5.1. A typical procedure for the synthesis of cinnamoyl chloride

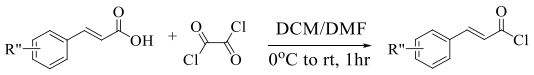

To a stirring solution of cinnamic acid (0.2 g, 1.10 mmol) and 2 drops DMF in anhydrous dichloromethane (DCM, 5 mL), oxalyl chloride (0.21g, 1.6 mmol) was added at 0 °C in an ice bath under nitrogen atmosphere. After 10 min, the reaction was stirred at room temperature for 50 min. The progression of the reaction was tracked by TLC. The crude product was dried under vacuum on rotavapor under N_2. The crude product was used for the next step without further purification.

10.6. A typical procedure for the synthesis of (E)-1-(4-(4-(4-methoxyphenyl)-6-(p-tolyl) pyrimidine-2-yl)piperazin-1-yl)-3-phenylprop-2-en-1-one (8a-n)

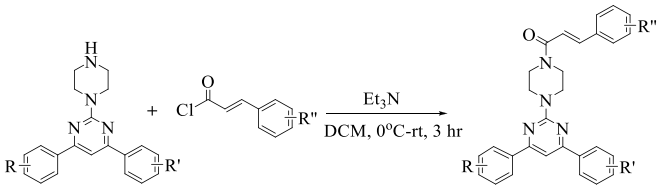

4,6-diphenyl-2-(piperazin-1-yl) pyrimidine **5** (0.2 g, 0.63 mmol) dissolved in DCM (3 mL) was added to a stirring solution of cinnamoyl chloride **7** (0.16g, 0.95 mmol) and Et_3N (0.3 eq.) in DCM (5 mL) at 0°C under N_2. After 10 min, the reaction mixture was allowed to stir for 3 h at room temperature under N_2. The progression of the reaction was tracked using TLC. After completion of the reaction, solvent was evoparated under reduced pressure. The obtained crude compound was purified by column chromatography using DCM (100 %) as an eluent to obtain the following pure compounds.

10.6.1. Spectral data for compound 8 (a-r)

(E)-1-(4-(4-(4-chlorophenyl)-6-(4-methoxyphenyl)pyrimidin-2-yl*) piperazin*-1-yl*)-3-phenylprop-2-en-1-one* (**8a**): Yellow solid, yield: 86 %, mp = 216–219 °C; FT-IR (ATR, ν_{max}, cm^{-1}): ν = 2950-2840 (C-H, CH_3), 1676-1624 (C=C, olefin), 1282 (C-O, OCH_3), 983 (C=C, alkene), ^1H NMR (400 MHz, DMSO-d_6, δ, ppm): 8.33 (d, J = 8.58 Hz, 2H, ArH), 8.29 (d, J = 8.81 Hz, 2H, ArH), 7.80 (s, 1H, ArH), 7.75 (d, = 8.57 Hz, 2H, ArH), 7.60 (d, J = 8.57 Hz, 2H, ArH), 7.55 (d, J = 15.44 Hz, 1H, Ph-C**H**=CH), 7.44–7.40 (m, 3H, ArH), 7.35 (d, J = 15.40 Hz, 1H, Ph-CH=C**H**), 7.08 (d, J = 8.84 Hz, 2H, ArH), 3.98 (s.br, 4H, $2CH_2$), 3.85 (s, 3H, OCH_3), 3.85–3.74 (m. 4H, $2CH_2$); ^{13}C NMR (100 MHz, DSMO-d_6, δ ppm): 164.63, 164.35, 162.91, 161.54, 161.43, 141.61, 136.12, 135.37, 135.14, 129.54, 129.34, 128.82, 128.75, 128.67, 128.01, 118.26, 114.02, 100.90, 55.35 (OCH_3); HRMS (ESI, *m/z*) $[M+H]^+$; calculated for $C_{30}H_{27}ClN_4O_2$, 511.1901. Found 511.1896.

(E)-1-(4-(4-(4-chlorophenyl)-6-(4-methoxyphenyl)pyrimidin-2-yl*) piperazin*-1-yl*)-3-(p-tolyl)prop-2-en-1-one* (**8b**): Yellow solid, yield: 88 %, mp = 207–209 °C; I.R. FT-IR (ATR, ν_{max}, cm^{-1}): ν =2994.33 (C-H, olefin), 2916.03, 2834.98 (C-H, CH_3), 1649.56 (C=C, olefin), 783.05 (C-Cl). ^1H NMR (400 MHz, $CDCl_3$, δ, ppm): 8.07 (dd, J = 15.64 Hz, 8.77 Hz, 4H, ArH), 7.71 (d, J = 15.91 Hz, 1H, Ph-C**H**=CH), 7.47–7.44 (m, 4H, ArH), 7.35 (s, 1H, ArH), 7.20 (d, J = 7.94 Hz, 2H, ArH), 7.01 (d, J = 8.89 Hz, 2H, ArH), 6.90 (d, J = 15.40 Hz, 1H, Ph-C**H**=CH), 4.09 (s.br, 4H, $2CH_2$), 3.88 (s, 3H, OCH_3), 3.80 (s.br, 4H, $2CH_2$) 2.38 (s, 3H, CH_3); ^{13}C NMR (100 MHz, DMSO-d_6, δ ppm): 164.96, 164.73, 164.59, 161.95, 151.70, 149.32, 147.13, 140.66, 135.37, 134.064, 134.048, 130.27,

130.22, 129.25, 128.52, 127.63, 120.85, 119.69, 112.04, 110.89, 101.45, 56.20 (OCH_3), 28.55 (CH_3); HRMS (ESI, *m/z*) $[M+H]^+$; calculated for $C_{31}H_{29}ClN_4O_3$, 525.2057.

(E)-1-(4-(4-(4-methoxyphenyl)-6-(p-tolyl)pyrimidin-2-yl*)piperazin*-1-yl*)-3-phenylprop-2-en-1-one* (**8c**): Creamy white solid, yield: 90 %, mp = 185–187 °C; FT-IR (ATR, ν_{max}, cm^{-1}): ν = 3010 (C-H of Olefin), 2997-2840 (C-H of CH_3), 1643-1605 (C=C OF Ar), 1251 (C-O, OCH_3), 980 (C-H of Olefin); ^1H NMR (400 MHz, $CDCl_3$, δ, ppm): 8.10 (d, J = 8.90 Hz, 2H, ArH), 8.02 (d, J = 8.19 Hz, 2H, ArH), 7.73 (d, J = 15.43 Hz, 1H, Ph-C**H**=CH), 7.57–7.55 (m, 1H, ArH), 7.40–7.38 (m, 4H, ArH), 7.30 (d, J = 7.99 Hz, 2H, ArH), 7.01 (d, J = 8.89 Hz, 2H, ArH), 6.96 (d, J = 15.43 Hz, 1H, Ph-CH=C**H**), 4.10 (s.br, 4H, $2CH_2$), 3.89 (s. 3H, OCH_3), 2.43 (s, 3H, CH_3); ^{13}C NMR (100 MHz, DSMO-d_6, δ ppm): 164.61, 164.11, 163.98, 161.47, 161.41, 141.60, 140.44, 135.14, 134.50, 129.55, 129.51, 129.03, 128.76, 128.76, 128.68, 128.53, 128.02, 12.97, 118.26, 114.00, 100.61, 55.34(OCH_3), 20.98 (CH_3); HRMS (ESI, *m/z*) $[M+H]^+$; calculated for $C_{31}H_{30}N_4O_2$, 513.2267; Found 513.2272.

(E)-3-(4-chlorophenyl)-1-(4-(4-(4-methoxyphenyl)-6-(p-tolyl)pyrimidin-2-yl*)piperazin*-1-yl*)prop-2-en-1-one* (**8d**): Brown solid, yield: 71 %, mp = 169–172 °C; FT-IR (ATR, ν_{max}, cm^{-1}): ν = 3128 (C-C, Olefin), 2938-2840 (C-H, CH_3), 1607 (C=C, olefin), 1212.33–1236.35 (C-O, OCH_3), 980 (C-C, Olefin); ^1H NMR (400 MHz, $CDCl_3$, δ, ppm): 8.11–8.08 (d, J = 8.90 Hz, 2H, ArH), 8.01 (d, J = 8.18 Hz, 2H, ArH), 7.67 (d, J = 15.43 Hz, 1H, Ph-C**H**=CH), 7.48 (d, J = 8.46 Hz, 2H, ArH), 7.38–7.35 (m, 3H, ArH), 7.30 (d, J = 7.96 Hz, 2H, ArH), 7.01 (d, J = 8.89 Hz, 2H, ArH), 6.92 (d, J = 15.43 Hz, 1H, Ph-CH=C**H**), 4.10 (s.br, 4H, $2CH_2$), 3.88 (s, 3H, CH_3), 3.80 (s.br, 4H, $2CH_2$), 2.43 (s, 3H, CH_3); ^{13}C NMR (100 MHz, $CDCl_3$, δ ppm): 164.43, 165.06, 164.70, 161.99, 161.65, 141.61, 140.69, 135.50, 135.50, 135.29, 133.21, 131.48, 129.42, 129.10, 128.99, 128.88, 128.68, 128.58, 126.58, 117.69, 114.04, 113.35, 101.54, 55.43 (OCH_3), 21.45 (CH_3); HRMS (ESI, *m/z*) $[M+H]^+$; calculated for $C_{31}H_{29}ClN_4O_3$, 525.2057.

(E)-3-(3,4-dimethoxyphenyl)-1-(4-(4-(4-methoxyphenyl)-6-(p-tolyl) pyrimidin-2-yl*)piperazin*-1-yl*)prop-2-en-1-one* (**8e**): Creamy white solid, yield: 93 %, mp = 124–128 °C; FT-IR (ATR, ν_{max}, cm^{-1}: ν = 2996.75 (C-H, olefin), 2911.69–2836.59 (C-H, CH_3), 1723.52, 1643.39 (C=C, olefin), 1237.32 (C-O, OCH_3); ^1H NMR (400 MHz, $CDCl_3$, δ, ppm): 8.11–8.08 (d, J = 8.90 Hz, 2H, ArH), 8.01 (d, J = 8.19 Hz, 2H, ArH), 7.68 (d, J = 15.32 Hz, 1H, Ph-C**H**=CH), 7.38 (s, 1H, ArH), 7.30 (d, J = 7.99 Hz, 2H, ArH), 7.15–7.13 (m, 2H, ArH), 7.06 (d, J = 1.89 Hz, 1H, ArH), 7.00 (d, J = 8.87 Hz, 2H, ArH), 6.88 (d, J = 8.33 Hz, 1H, ArH), 6.81 (d, J = 15.32 Hz, 1H, Ph-CH=C**H**), 4.10 (s.br, 4H, $2CH_2$), 3.94 (s. 3H, OCH_3) 3.92 (s. 3H, OCH_3) 3.88 (s. 3H, OCH_3) 3.83 (s.br, 4H, $2CH_2$) 2.43 (s, 3H, CH_3); HRMS (ESI, *m/z*) $[M+H]^+$; calculated for $C_{33}H_{34}N_4O_4$, 551.2658.

(E)-1-(4-(4,6-bis(4-methoxyphenyl)pyrimidin-2-yl*)piperazin*-1-yl*)-3-phenylprop-2-en-1-one* (**8f**): Creamy white solid, yield: 86 %, mp = 170–172 °C; FT-IR (ATR, ν_{max}, cm^{-1}): 3005 (C-H, olefin), 2929–2940 (C-H, CH_3), 1646-1606 (C=C, olefin), 1265 (C-O, OCH_3), 983 (C-C, Olefin); ^1H NMR (400 MHz, $CDCl_3$, δ, ppm): 8.10 (d, J = 8.88 Hz, 4H, ArH), 7.74 (d, J = 15.45 Hz, 1H, Ph-C**H**=CH), 7.56–7.55 (m, 1H, ArH), 7.40–7.35 (m, 3H, ArH), 7.01 (d, J = 8.92 Hz, 4H, ArH), 6.96 (d, J = 15.41 Hz, 1H, Ph-CH=C**H**), 4.10 (s.br, 4H, $2CH_2$), 3.88 (s, 6H, OCH_3), 3.80 (s.br, 4H, $2CH_2$); ^{13}C NMR (100 MHz, $CDCl_3$, δ ppm): 165.77, 164.58, 161.97, 161.61, 143.03, 135.29, 130.55, 129.70, 128.85, 128.56, 127.82, 117.12, 114.03, 101.04, 55.43 ($2OCH_3$). ; HRMS (ESI, *m/z*) $[M+H]^+$; calculated for $C_{31}H_{30}N_4O_3$, 507.2396. Found 507.2396.

(E)-1-(4-(4,6-bis(4-methoxyphenyl)pyrimidin-2-yl*)piperazin*-1-yl*)-3-(4-chlorophenyl)prop-2-en-1-one* (**8g**): Yellow solid, yield: 89 %, mp = 169–172 °C; FT-IR (ATR, ν_{max}, cm^{-1}): ν = 3003.37 (C-H, Olefin), 2931-2840 (C-H, CH_3), 1714 (C=O), 1650 (C=C, Ar), 1254, 1236 (C-O, OCH_3), 784 (C-Cl).^1H NMR (400 MHz, DMSO-d_6, δ, ppm): 8.27 (d, J = 8.36 Hz, 4H, ArH), 7.81–7.78 (m, 2H, ArH), 7.72 (s, 1H, ArH), 7.56–7.48 (m, 3H, ArH), 7.38 (d, J = 15.42 Hz, 1H, Ph-CH=C**H**), 7.08 (d, J = 8.36 Hz, 4H, ArH), 3.98 (s.br, 4H, $2CH_2$) 3.85 (s, 6H, $2CH_3$), 3.75 (s.br, 4H, $2CH_2$); ^{13}C NMR (100 MHz, DMSO-d_6, δ ppm): 164.46, 163.83, 161.47, 161.40, 140.22, 134.16, 134.01, 130.07, 129.78, 128.80, 128.68, 119.19, 114.02, 100.23, 55.36 ($2OCH_3$); HRMS (ESI, *m/z*) $[M+H]^+$; calculated for $C_{31}H_{29}ClN_4O_3$, 541.2006. Found 541.2002.

(E)-1-(4-(4,6-bis(4-methoxyphenyl)pyrimidin-2-yl*)piperazin*-1-yl*)-3-(p-tolyl)prop-2-en-1-one* (**8h**): Creamy white solid, yield: 74 %, mp = 172–174 °C; FT-IR (ATR, ν_{max}, cm^{-1}): ν = 2995-2840 (C-H, CH_3), 1643-1606 (C=C, olefin), 1234 (C-O, OCH_3), 980 (C-C, Olefin); ^1H NMR (400 MHz, DMSO-d_6, δ, ppm): 8.27 (d, J = 8.66 Hz, 4H, ArH), 7.72 (s, 1H, ArH), 7.64 (d, J = 7.85 Hz, 2H, Ar), 7.52 (d, J = 15.34 Hz, 1H, Ph-C**H**=CH), 7.30 (s, 1H, ArH), 7.26–7.22 (m, 2H, ArH), 7.08 (d, J = 8.74 Hz, 4H, ArH), 3.97 (s.br, 4H, $2CH_2$), 3.85 (s. 6H, $2OCH_3$) 3.74–3.64 (m, 4H, $2CH_2$); ^{13}C NMR (100 MHz, DMSO-d_6, δ ppm): 164.74, 163.80, 161.44, 161.38, 141.64, 139.33, 132.42, 129.37, 129.12, 128.66, 128.23, 128.03, 117.11, 114.00, 100.19, 55.35 (OCH_3), 20.97 (CH_3); HRMS (ESI, *m/z*) $[M+H]^+$; calculated for $C_{32}H_{32}N_4O_3$, 521.2552. Found 521.2552.

(E)-1-(4-(4,6-bis(4-methoxyphenyl)pyrimidin-2-yl*)piperazin*-1-yl*)-3-(4-methoxyphenyl)prop-2-en-1-one* (**8i**): Brown solid, yield: 71 %, FT-IR (ATR, ν_{max}, cm^{-1}): ν = 3127 (C-C, olefin), 2930-2848 (C-H, CH_3), 1653 (C=C, olefin), 1258 (C-O, OCH_3), 986(C-C, olefin); ^1H NMR (400 MHz, $CDCl_3$, δ, ppm): 8.10–8.08 (d, J = 8.87 Hz, 4H, ArH), 7.72–7.68 (d, J = 15.35 Hz, 1H, Ph-C**H**=CH), 7.52–7.49 (d, J = 8.70 Hz, 2H, ArH), 7.34 (s, 1H, ArH), 7.02–6.70 (d, J = 8.87 Hz, 4H, ArH), 6.92–6.90 (d, J = 8.73 Hz, 2H, ArH), 6.84–6.80 (d, J = 15.35 Hz, 1H, Ph-CH=C**H**), 4.09 (s,br.4H, $2CH_2$), 3.88 (s, 6H, $2OCH_3$), 3.84 (s, 3H, OCH_3), 3.81 (s.br, 4H, $2CH_2$); ^{13}C NMR (100 MHz, $CDCl_3$, δ ppm): 166.03, 164.57, 161.60, 142.72, 130.58, 129.39, 128.88, 128.03, 114.59, 114.27, 114.02, 101.00, 55.43($2OCH_3$), 55.38 (OCH_3); HRMS (ESI, *m/z*) $[M+H]^+$; calculated for $C_{32}H_{32}N_4O_4$, 537.2502.

(E)-1-(4-(4,6-bis(4-methoxyphenyl)pyrimidin-2-yl*)piperazin*-1-yl*)-3-(3,4-dimethoxyphenyl)prop-2-en-1-one* (**8j**): Yellow solid, yield: 81 %, mp = 116–118 °C; FT-IR (ATR, ν_{max}, cm^{-1}): ν =2998 (C-H, Olefin), 2929-2836 (C-H, CH_3), 1643. (C=C, of Ar), 1234 (C-O, OCH_3); ^1H NMR (400 MHz, DMSO-d_6, δ, ppm): 8.27 (d, J = 8.38 Hz, 4H, ArH), 7.73 (s, 1H, ArH), 7.50 (d, J = 15.22 Hz, 1H, Ph-C**H**=CH), 7.40 (s, 1H, ArH), 7.24–7.19 (m, 2H, ArH), 7.08 (d, J = 8.80 Hz, 4H, ArH), 6.98 (d, J = 8.28 Hz, 1H, ArH), 3.98 (s.br, 4H, $2CH_2$) 3.85–3.72 (m, 16H, $2CH_3$, $4CH_3$); ^{13}C NMR (100 MHz, DMSO-d_6, δ ppm): 167.11, 164.91, 163.81, 161.40, 150.32, 142.01, 129.61, 129.54, 128.68, 127.98, 122.47, 121.51, 115.55, 114.01, 111.61, 110.24, 100.17, 55.69 (OCH_3), 55.55 (OCH_3), 55.44 (OCH_3), 55.36 (OCH_3); HRMS (ESI, *m/z*) $[M+H]^+$; calculated for $C_{33}H_{34}N_4O_5$, 567.2607. Found 567.2605.

(E)-1-(4-(4,6-bis(4-methoxyphenyl)pyrimidin-2-yl*)piperazin*-1-yl*)-3-(furan*-2-yl*)prop-2-en-1-one* (**8k**): Yellow solid, yield: 91 %, mp = 176–178 °C; FT-IR (ATR, ν_{max}, cm^{-1}): ν = 3060 (C-H, olefin), 2935-2842 (C-H, CH_3), 1658 (C=C, olefin), 1260 (C-O, OCH_3), 988 (C-C, Olefin); ^1H NMR (400 MHz, $CDCl_3$, δ, ppm): 8.09 (d, J = 8.85 Hz, 4H, ArH), 7.52 (d, J = 15.08 Hz, 1H, Ph-C**H**=CH), 7.47 (s, 1H, ArH), 7.34 (s, 1H, ArH), 7.01 (d, J = 8.86 Hz, 4H, ArH), 7.94 (d, J = 15.91 Hz, 1H, Ph-C**H**=CH), 7.81 (d, J = 8.48Hz, 2H, ArH), 6.88 (d, J = 15.08 Hz, 1H, Ph-CH=C**H**), 6.57 (d, J = 3.32 Hz, 1H, ArH), 6.47 (dd, J = 1.72 Hz, 1H, ArH), 4.08 (s, 4H, $2CH_2$), 3.88 (s. 6H, OCH_3), 3.79 (s.br, 4H, $2CH_2$); ^{13}C NMR (100 MHz, $CDCl_3$, δ ppm):165.47, 164.57, 161.97, 161.60, 151.71, 143.95, 130.56, 129.82, 128.55, 114.53, 114.02, 113.92, 112.23, 101.00, 55.42 ($2OCH_3$); HRMS (ESI, *m/z*) $[M+Na]^+$; calculated for $C_{31}H_{29}ClN_4O_3$, 497.2189; Found 497.2186.

(E)-1-(4-(4-(3,4-dimethoxyphenyl)-6-(4-ethylphenyl)pyrimidin-2-yl*) piperazin*-1-yl*)-3-phenylprop-2-en-1-one* (**8l**): Creamy white solid, yield: 92 %, mp = 174–176 °C; FT-IR (ATR, ν_{max}, cm^{-1}): 2997-2856 (C-H, CH_3), 1646 (C=C, olefin), 1264 (C-O, OCH_3), 982 (C-C, Olefin), NMR (400 MHz, $CDCl_3$, δ, ppm): 8.20 (d, J = 7.91 Hz, 2H, ArH), 7.90 (d, J = 8.49 Hz, 1H, ArH), 7.84 (s, 1H, ArH), 7.75–7.74 (m, 3H, ArH), 7.55 (d, J = 15.34 Hz, 1H, Ph-C**H**=CH), 7.43–7.33 (m, 6H, ArH) 7.08 (d, J = 8.44 Hz, 1H, ArH), 3.99 (s,br, 4H, $2CH_2$), 3.90 (s, 3H, CH_3), 3.85(s, 3H, CH_3), 3.85–3.76 (m, 4H, $2CH_2$), 2.68(qt, J = 7.58 Hz, 2H, CH_2), 1.23(t, J = 7.59 Hz, 3H, CH_3); ^{13}C NMR (100 MHz, DMSO-d_6, δ ppm): 165.17, 164.74, 164.60(C=O), 151.71, 149.32, 147.13, 142.09, 135.67, 135.38,

130.28, 130.02, 129.24, 128.52, 128.50, 127.63, 120.86, 118.81, 112.05, 110.91, 101.44, 56.26 ($2OCH_3$), 56.26 ($2CH_2$), 28.56 ($2CH_2$), 15.91 (CH_2), HRMS (ESI, *m/z*) [M+H]+; calculated for $C_{33}H_{34}N_4O_3$, 535.2709.

(E)-3-(4-chlorophenyl)-1-(4-(4-(3,4-dimethoxyphenyl)-6-(4-ethylphenyl)pyrimidin-2-yl)piperazin-1-yl)prop-2-en-1-one (**8m**): Creamy white fluffy solid, yield: 79 %, mp = 109–110 °C; FT-IR (ATR, ν_{max}, cm^{-1}): ν = 2965-2836 (C-H, CH_3), 1649-1613 (C=C, olefin), 1260 (C-O, OCH_3), 982 (C=C, alkene); ^{1}H NMR (400 MHz, DMSO-d_6, δ, ppm): 8.22–8.20 (d, *J* = 8.25 Hz, 2H, ArH), 7.93–7.90 (dd, *J* = 8.47Hz, 1.97 Hz, 1H, ArH), 7.80–7.78 (d, *J* = 8.54 Hz, 2H, ArH), 7.75 (s, 1H, ArH), 7.56–7.52 (d, *J* = 15.39 Hz, 1H, Ph-CH=C**H**), 7.49–7.47 (d, *J* = 8.51 Hz, 2H, ArH), 7.40 (s, 1H, ArH), 7.38–7.36 (d, *J* = 8.00 Hz, 2H, ArH), 7.10–7.08 (d, *J* = 8.54 Hz, 1H, ArH), 3.98 (s.br, 4H, $2CH_2$), 3.90 (s, 3H, CH_3), 3.85 (s, 3H, CH_3), 3.75 (s.br, 4H, $2CH_2$) 2.69 (q, *J* = 7.56 Hz, 2H, CH_2), 1.22 (t, *J* = 7.61 Hz, 3H, CH_3); ^{13}C NMR (100 MHz, DMSO-d_6, δ ppm):164.44, 164.21, 164.08, 161.44, 151.17, 148.79, 146.66, 140.21, 134.84, 134.15, 133.99, 129.77, 129.71, 128.77, 128.06, 127.15, 120.35, 119.17, 111.49, 110.29, 100.94, 55.68 (OCH_3), 55.62 (OCH_3), 28.07 (CH_2), 15.47 (CH_3); HRMS (ESI, *m/z*) $[M+H]^+$; calculated for $C_{33}H_{33}ClN_4O_3$, 569.2319. Found 569.2314.

(E)-1-(4-(4-(3,4-dimethoxyphenyl)-6-(4-ethylphenyl)pyrimidin-2-yl)piperazin-1-yl)-3-(p-tolyl)prop-2-en-1-one (**8n**): Creamy white solid, yield: 87 %, mp = 159–161 °C; FT-IR (ATR, ν_{max}, cm^{-1}): 3080 (C-H, olefin), 3003-2835 (C-H, CH_3), 1771-1712 (C=O), 1652 1606 (C=C, olefin), 1257 (C-O, OCH_3), 981 (C-C, Olefin); ^{1}H NMR (400 MHz, $CDCl_3$, δ, ppm): 8.04 (d, *J* = 8.16 Hz, 2H, ArH), 7.73–7.69 (m, 3H, ArH), 7.45 (d, *J* = 8.05 Hz, 1H, ArH), 7.33 (d, *J* = 8.12 Hz, 2H, ArH), 7.20 (d, *J* = 7.95 Hz, 2H, ArH), 6.98 (d, *J* = 8.35 Hz, 1H, ArH), 6.91 (d, *J* = 15.36 Hz, 1H, Ph-C**H**=CH), 4.10 (s,br, 4H, $2CH_2$), 4.01 (s, 3H, OCH_3), 3.96 (s, 3H, OCH_3), 3.80, (s,br, 4H, $2CH_2$), 2.68(qt, *J* = 7.59 Hz, 2H, CH_2), 1.22(t, *J* = 7.58 Hz, 3H, CH_3); ^{13}C NMR (100 MHz, DMSO-d_6, δ ppm):164.75, 164.21, 164.08, 161.44, 151.17, 148.79, 146.65, 141.66, 139.32, 134.86, 132.42, 129.73, 129.36, 128.03, 127.15, 120.35, 117.10, 111.49, 110.30, 100.92, 55.68 (OCH_3), 55.61 (OCH_3), 28.89 (CH_2), 20.96 (CH_2), 15.47 (CH_3); HRMS (ESI, *m/z*) $[M+H]^+$; calculated for $C_{34}H_{36}N_4O_3$, 549.2865. Found 549.2867.

(E)-1-(4-(4-(3,4-dimethoxyphenyl)-6-(4-ethylphenyl)pyrimidin-2-yl)piperazin-1-yl)-3-(4-methoxyphenyl)prop-2-en-1-one (**8o**): Creamy white fluffy solid, yield: 89 %, mp = 114–116 °C; FT-IR (ATR, ν_{max}, cm^{-1}): ν= 3080 (C-C, Olefin), 2934–3840 (C-H, CH_3), 1603 (C=C, of Ar), 1259 (C-O, OCH3), 980 (C-C, Olefin); ^{1}H NMR (400 MHz, DMSO-d_6, δ, ppm): 8.20 (d, *J* = 7.57 Hz, 2H, ArH), 7.90 (d, *J* = 8.37 Hz, 1H, ArH), 7.86 (s, 1H, ArH), 7.74 (s, 1H, ArH), 7.69 (d, *J* = 8.02 Hz, 2H, ArH), 7.51 (d, *J* = 15.25 Hz, 1H, Ph-C**H**=CH), 7.36 (d, *J* = 7.59 Hz, 2H, ArH), 7.18 (d, *J* = 15.32 Hz, 1H, Ph-CH=C**H**), 7.09 (d, *J* = 8.69Hz, 1H, ArH), 6.97 (d, *J* = 7.69 Hz, 2H, ArH), 3.98 (s,br, 4H, $2CH_2$), 3.90 (s, 3H, OCH_3), 3.85 (s, 3H, OCH_3), 3.80 (s, 3H, OCH_3), 3.75–3.71 (m, 4H, $2CH_2$), 2.69 (q, *J* = 7.47 Hz, 2H, CH_2), 1.23(*t*, *J* = 7.53 Hz, 3H, CH_3); ^{13}C NMR (100 MHz, DMSO-d_6, δ ppm): 164.89, 164.20, 164.07, 161.44,160.42, 151.17, 148.79, 146.61, 141.43, 134.85, 129.75, 129.63, 129.19, 128.00, 127.77, 127.32, 127.10, 120.33, 115.58, 114.17, 111.52, 110.37, 100.90, 55.69 (OCH_3), 55.60 (OCH_3), 55.23 (OCH_3), 15.39 (CH_2), 15.36 (CH_3); HRMS (ESI, *m/z*) [M+H]+; calculated for $C_{34}H_{36}N_4O_4$, 565.2815.

(E)-1-(4-(4-(3,4-dimethoxyphenyl)-6-(4-ethylphenyl)pyrimidin-2-yl)piperazin-1-yl)-3-(furan-2-yl)prop-2-en-1-one (**8p**): Creamy white fluffy solid, yield: 86 %, mp = 179–182 °C; FT-IR (ATR, ν_{max}, cm^{-1}): ν = 2938-2840 (C-H, CH_3), 1256 (C-O), 984 (C-C, Olefin); ^{1}H NMR (400 MHz, DMSO-d_6, δ, ppm): 8.20 (d, *J* = 8.24 Hz, 2H, ArH), 7.91 (dd, *J* = 8.49 Hz, 1.91 Hz, 1H, ArH), 7.82 (dd, *J* = 10.40 Hz, 1.93 Hz, 1H, ArH), 7.75 (s, 2H, ArH), 7.41–7.36 (m, 3H, ArH), 7.09 (d, *J* = 8.54 Hz, 1H, ArH), 7.00 (d, *J* = 15.24 Hz, 1H, Ph-CH=C**H**), 6.88 (d, *J* = 3.32 Hz, 1H, ArH), 6.62 (dd, *J* = 1.71 Hz, 1H, ArH), 3.97(s.br, 4H, $2CH_2$), 3.90 (s. 3H, OCH_3) 3.84 (s. 3H, OCH_3), 3.84 (s.br, 4H, $2CH_2$) 2.69 (q, *J* = 7.54 Hz, 2H, CH_2), 1.23 (t, *J* = 7.57 Hz, 3H, CH_3); ^{13}C NMR (100 MHz, DMSO-d_6, δ ppm):165.75, 165.49, 165.18, 164.74, 162.01, 151.69, 151.22, 149.16, 147.04, 143.95, 143.03, 135.56, 130.88, 129.85, 128.84, 128.25, 127.81, 127.123, 120.22, 114.49, 113.96, 112.24, 110.97, 110.04, 101.77, 55.04, 25.82, 15.51; HRMS (ESI, *m/z*) $[M+H]^+$; calculated for $C_{31}H_{32}N_4O_4$, 525.2502.

(E)-1-(4-(4-(4-chlorophenyl)-6-(pyridin-3-yl)pyrimidin-2-yl)piperazin-1-yl)-3-(p-tolyl)prop-2-en-1-one (**8q**): Yellow solid, yield: 84 %, mp = 172–174 °C; FT-IR (ATR, ν_{max}, cm^{-1}): ν = 3080.95 (C-H, olefin), 2997-2859(C-H, CH_3), 1640 (C=O), 1242 (C-O), 982 (C-C, Olefin), 783(C-Cl, ArCl); ^{1}H NMR (400 MHz, DMSO-d_6, δ, ppm): 9.46 (s, 1H, ArH), 8.72 (d, *J* = 4.08 Hz, 1H, ArH), 8.62 (d, *J* = 7.89 Hz, 1H, ArH), 8.33 (d, *J* = 8.37 Hz, 2H, ArH), 7.94 (s, 1H, ArH), 7.63–7.55 (m, 5H, ArH), 7.51 (d, *J* = 15.34 Hz, 1H, Ph-C**H**=CH), 7.27 (d, *J* = 15.68 Hz, 1H, Ph-CH=C**H**), 7.22 (d, *J* = 7.69 Hz, 2H, ArH) 3.98(s.br, 4H, $2CH_2$), 3.87–3.74 (m. 4H, $2CH_2$) 2.33 (s, 3H, CH_3); ^{13}C NMR (100 MHz, DSMO-d_6, δ ppm): 164.79, 163.59, 162.79, 161.45, 151.44, 148.44, 141.69, 139.36, 135.75, 135.73, 134.57, 132.55, 132.40, 129.49, 129.38, 129.12, 128.17, 128.02, 123.75, 118.07, 117.07, 101.89, 20.96 (CH_3); HRMS (ESI, *m/z*) $[M+H]^+$; calculated for $C_{29}H_{26}ClN_5O$, 496.1904; Found 496.2116.

(E)-1-(4-(4-(furan-3-yl)-6-(pyridin-3-yl)pyrimidin-2-yl)piperazin-1-yl)-3-phenylprop-2-en-1-one (**8r**): Yellow solid, yield: 89 %, mp = 163–165 °C; FT-IR (ATR, ν_{max}, cm^{-1}): ν = 3077 (C-C, Olefin), 2932.13–2840 (C-H, CH_3), 1660 (C=C, olefin), 1259 (C-O, OCH_3); ^{1}H NMR (400 MHz, $CDCl_3$, δ, ppm): 9.30 (s, 1H, ArH), 8.73 (s, 1H, ArH), 8.40–8.38 (d, *J* = 7.97Hz, 2H, ArH), 8.06 (d, *J* = 8.57 Hz, 2H, ArH), 7.74 (d, *J* = 15.41 Hz, 1H, Ph-C**H**=CH), 7.56–7.54 (m, 2H, ArH), 7.48 (d, *J* = 8.57 Hz, 2H, ArH), 7.39 (d, *J* = 8.73 Hz, 4H, ArH), 6.95 (d, *J* = 15.42 Hz, 1H, Ph-CH=C**H**), 4.10 (s,br, 4H, $2CH_2$), 3.90–3.83 (m. 4H, $2CH_2$); ^{13}C NMR (100 MHz, $CDCl_3$, δ ppm): 165.76, 164.58, 163.22, 161.98, 151.33, 148.37, 143.24, 136.92, 136.01, 135.20, 134.51, 129.78, 129.03, 128.87, 128.43, 127.83, 123.59, 116.91, 102.02; HRMS (ESI, *m/z*) $[M+H]^+$; calculated for $C_{26}H_{23}N_5O_2$, 438.1930.

11. Pharmacological evaluation

11.1. Antimalarial activity

11.1.1. Drug sensitivity pLDH assay

The chloroquine-sensitive strain of *P. falciparum* (NF54) was maintained continuously *in vitro* in supplemented RPMI-1640 culture media at 37°C and gassed with a mixture of 5 % CO_2, 3 % O_2 and 92 % N_2 [45]. The culture was synchronized with 5 % D-sorbitol at the ring stage [45,46]. For determination of the antiplasmodial activity of different compounds, the synchronized ring-stage parasites were adjusted to a final parasitaemia of 2 % and 2 % haematocrit, to which serial dilutions of the derivatives and positive control, quinine were added after a 24 h incubation. Negative controls included uninfected erythrocytes and drug-free parasitized erythrocytes. Following a further 48 h incubation period, the plates were frozen at −70°C for 1 h and thawed for 2 h. Twenty-five microliters of lysate were transferred to a non-sterile plate, to which 100 μl Malstat™ and 20 μl nitroblue tetrazolium and phenazine ethosulphate (1:1) mixture was added to each well and incubated for 40 min at 37°C to quantify the parasite lactate dehydrogenase (pLDH) activity [46]. Thereafter, 5 % acetic acid was added to each well, and the absorbance of the formazan products was read at 620 nm as an indicator of parasite viability. The percentage of parasite viability, taking the appropriate controls into account, was calculated and used to determine the concentration required to inhibit parasite growth by 50 % (IC_{50} value) from log-sigmoid dose-response curves using the GraphPad Prism® 5.0.0 software. Each experiment was repeated at least in triplicate [35,47].

11.1.2. Stage dependant effect

In order to determine the specific effects of two of the more active compounds on the intra-erythrocytic asexual parasitic stages, a 48 h observational study was conducted. The synchronized ring-staged

parasite suspension (2 % parasitaemia and 2 % haematocrit) was incubated with the respective IC_{50} concentrations of these active compounds or quinine. An untreated parasite control was also prepared for comparison between treated and untreated parasites. The parasite cultures were all gassed with a mixture of 3 % oxygen, 4 % carbon dioxide and 93 % nitrogen for 30 s, sealed and placed in an incubator at 37 °C in a static position. Every 8 h, a Giemsa-stained thin blood smear was prepared for microscopic assessment and the flask re-gassed and returned to its 37 °C environment. The blood smears were analyzed microscopically at 1000x magnification using an Olympus® CX23 microscope and CellSens version 1.5 software (Olympus®, Japan) to determine total percentage parasitaemia and percentage of each parasite stage at each time interval. Any morphological changes to the parasites and infected RBCs were noted for each time interval over the 48 h period.

11.2. Toxicity assays

11.2.1. Cell viability assay

Human embryonic kidney epithelial (HEK-293) cells were maintained at 37°C in a humidified chamber with 5 % CO_2 as a monolayer in Dulbecco's modified Eagle's medium (DMEM) supplemented with 10 % of fetal bovine serum, 100 IU ml^{-1} penicillin and 100 μg ml^{-1} streptomycin. A cell suspension (10,000 cells per well) was incubated at 37°C for 48 h with serial dilutions of compounds/positive control. A final concentration of less than 1 % DMSO had no effect on the viability of the cells. Thereafter, 40 μl of (3-(4, 5-dimethylthiazolyl-2)-2, 5-diphenyltetrazolium bromide (MTT; 5 mg ml^{-1} in phosphate buffer saline (pH 7.3)) was added to each well and incubated for a further 2 h. DMSO was used to dissolve the formazan crystals and then quantified by reading the absorbance at 540 nm with a reference wavelength of 690 nm (Labsystems Multiskan RC) [48]. Percent cellular viability was determined using the appropriate controls and used to calculate the IC_{50} values, which were compared to the positive control, camptothecin. The experiment was repeated in triplicate [49,50].

11.2.2. Red blood lysis assay

A 2 % (v/v) haematocrit of washed human red blood cells were incubated with the test compounds and standard antimalarial control at 50 μM for 48 h at 37°C [51]. After 48 h, the 96-well plate was centrifuged at 252×*g* for 5 min before the supernatant was dilute 1:4 with phosphate buffered saline (pH 7.4). The phosphate buffered saline was prepared with 136.89 mM sodium chloride, 4.1 mM di-sodium hydrogen phosphate dihydrate, 4.02 mM potassium chloride, and 1.47 mM potassium dihydrogen phosphate in Milli-Q® deionised water. The absorbance of each well was read at 414 nm and the % haemolysis was determined taking the untreated negative and Triton X100 positive controls into account. Each experiment was repeated at least in triplicate.

11.3. Binding affinity assays using selected synthetic compounds against P. falciparum Hsp70

Ligand-compound interaction studies were undertaken to define a possible antiplasmodial mechanism of action. Heat shock proteins are essential to parasite survival, in this study, we investigated the *P. falciparum* heat shock protein 70s, PfHsp70-1 and PfHsp70-z as possible antiplasmodial "protein-compound" interactive partners. Recombinant PfHsp70-1 and PfHsp70-z were produced in *E. coli* with a 6x Histidine tag and purified using a nickel affinity protein purification using a previously described method [52]. Binding affinities between the ligand and selected compound were investigated by SPR analysis using the BioNavis™ 420A ILVES MP-SPR (BioNavis, Tampere, Finland) [53]. Degassed PBS Tween 20 (4.3 mM Na_2HPO_4, 1.4 mM KH_2PO_4, 137 mM NaCl, 3 mM KCl, 0.005 % (v/v) Tween 20, and 20 mM EDTA; pH 7.4) was used as a system running buffer. PfHsp70-1 and PfHsp70-z were immobilized as ligands at 0.5 μg/ml onto functionalized 3D carboxymethyl dextran sensor chips (CMD 3D 500L; BioNavis, Tampere, Finland). Immobilization of ligands was achieved through amine coupling after 1-ethyl-3-(3-dimethylaminopropyl) carbodiimide (EDC) [Sigma Aldrich, Germany] and N-hydroxy-succinimide (NHS) [Sigma Aldrich, Germany] activation following a protocol provided by the manufacturer (BioNavis, Tampere, Finland) to achieve <200 RUs. A reference channel without immobilized protein served as a control for non-specific binding and changes in refractive index. As analytes, compounds (Compounds **8o** and **8l**) were prepared in aliquots of 0, 1.25, 2.5, 5, 10 and 20 nM and injected three times at a flow rate of 50 μl/min into each flow cell. Injections with buffer only were used as controls. Association between ligands and compounds was allowed for 3 min, and dissociation was monitored for a total of 10 min. Kinetics steady-state equilibrium constant data was processed after double referencing the sensograms and concatenating the responses of all five analyte concentrations by global fitting using TraceDrawer software version 1.8 (Ridgeview Instruments, Sweden).

12. Molecular docking

The Homology model of NBD of PfHsp70-1 (PlasmoDB accession number: PF3D7_0818900), and PfHsp70-z (PlasmoDB accession number: PF3D7_0708800.1) were built using Swiss model software [54]. The best sequence identity of 75.59 % and coverage of 0.82 was used for PfHsp70-1 (3c7n.1.B), while the best sequence identity for PfHsp70-z (3c7n.1.B) is 26.29 % with the coverage of 0.62. The compounds were minimized using the steepest descent method and GAFF force field add-on in Avogadro [55]. The systems were subjected to molecular docking using the predicted active site using Swiss dock software [56]. The pose with the lowest negative value was chosen based on the interactions and binding affinities of the ligands. All the compounds were docked using AutoDockTools-1.5.6 graphical user interface via the GitBash terminal [57] to define the grid box for the active site for PfHsp70-1, the spacing of 1 Å and centre (25.80 x 35.41 x11.10) and size (24 x 24 x 20) pointing in x, y, and z directions. Similarly, the grid box for the active site of PfHsp70-z has a centre (−16.09 x 46.48 x −18.15) and size (22 x 20 x 22) with a spacing of 1 Å pointing in x, y, and z directions, respectively. Docking calculations using the Lamarckian genetic algorithm were performed with AutoDock Vina [58]. Using UCSF ChimeraTools, atom types were assigned, Gasteiger charges were added to the compounds, and non-polar hydrogen on carbon atoms was merged. The water molecules were removed from the protein and added polar hydrogen, and the compounds docked into the active site of the two proteins. Finally, docking was validated based on the lowest energy pose, and the four compound systems were then subjected to molecular dynamics simulations.

13. Molecular dynamic (M.D.) simulations

We performed the M.D. simulations using the GPU version of the PMEMD.CUDA engine provided the AMBER package, FF18SB variant of the AMBER force field used to describe the protein [58]. By applying the restrained electrostatic potential (RESP) and the GENERAL AMBER Force Field (GAFF) procedures, partial charges were added to the compounds in ANTECHAMBER 18. The LEAP module in AMBER 18 was used to neutralize and solvate the free-bound and unbound systems by adding hydrogen atoms [H^+], sodium ions [Na^+], and chloride [Cl^-] counter ions. The amino acids were numbered numbering residues 1–547 for PfHsp70-1 and 1–658 for PfHsp70-z.

Additionally, all atom's explicit solvation was performed in an orthorhombic TIP3P box of water molecule size 10 Å. The procedure considered an initial minimization of 2500 steps with an applied restrained potential of 500 kcal mol^{-1}. Additional 5000 steps of full minimization were carried out by the conjugate algorithm without restraining conditions. The systems were gradually heated, starting from 0 to 300 K for 50 ps to maintain a fixed number of atoms and volumes,

considering a canonical ensemble (NVT). Following heating, an equilibration estimating 500 ps of each system was conducted; the operating temperature was kept constant at 300 K. Using 1 bar pressure provided by the Barendsen-barostat, the SHAKE algorithm was utilized to constrict the hydrogen bond constraint [59,60]. The total time for the M. D. simulation was 100 ns with a time step of 2 fs using a constant pressure of 1 bar, 300 K, and a Langevin thermostat [61]. The coordinates for PfHsp70-1, PfHsp70-1 and the bound systems were each saved every 1 ps, and the trajectories were analyzed using the CPTRAJ and PTRAJ modules in AMBER 18/GPU. The trajectories were analyzed for RMSD, RMSF, RoG, and Solvent accessible surface area (SASA) using CPPTRAJ. The structural and visual analysis [62] was done by employing the graphical user interface of UCSF Chimera and Discovery Studio 2019 client to analyze the binding mechanism of the ligand-bound systems [61], while the data was plotted with MicroCal Origin 6.0 data analysis software [63].

14. Binding free energy calculation

To estimate and compare the binding affinity of the systems, the free binding energy (BFE) was calculated using the Molecular Mechanics/GB Surface Area method (MM/GBSA) [71]. The energies considered over 100,000 snapshots from the 100 ns trajectories. The free binding energy (DG) calculated for each molecular species (complex, ligand, and receptor) can be expressed thus as:

$$\Delta G_{bind} = \Delta G_{complex} - \Delta G_{receptor} - \Delta G_{ligand}$$

$$\Delta G_{bind} = E_{gas} + G_{sol} - T\Delta S$$

$$E_{gas} = E_{int} + E_{vdw} + E_{ele}$$

$$G_{sol} + G_{GB} + G_{SA}$$

$$G_{SA} + \gamma SASA$$

Egas signifies the gas-phase energy, which consists of internal energy (E_{int}), Coulomb (Eele), and van der Waals energy (E_{vdW}). The E_{gas} was directly estimated from the FF18SB force field terms. Polar and non-polar states' energy contributions accounted for the solvation-free energy, G_{sol}. The non-polar solvation energy, SA. G_{SA} was determined from the solvent-accessible surface area (SASA) using a water probe radius of 1.4 A. In contrast, the polar solvation, G_{GB}, was obtained by solving the GB expression. S denotes the total entropy, and T is the system's temperature. The contribution of each residue to the total binding free energy obtained at the predicted active site by carrying out per-residue energy decomposition at the atomic level using the MM/GBSA method in AMBER 18 [64].

CRediT authorship contribution statement

Francis Kayamba: Writing – original draft, Methodology, Investigation, Data curation, Conceptualization. **Rajshekhar Karpoormath:** Conceptualization, Data curation, Formal analysis, Funding acquisition, Investigation, Methodology, Project administration, Resources, Supervision, Validation, Visualization. **Vincent A. Obakachi:** Writing – original draft, Software. **Mavela Mahlalela:** Writing – review & editing. **Danny Banda:** Writing – review & editing, Formal analysis. **Robyn L. van Zyl:** Validation, Resources, Data curation, Writing–original draft, Writing – original draft, Writing–review & editing. **Sahil Lala:** Investigation, Formal analysis, Data curation. **Tawanda Zininga:** Writing – review & editing, Validation, Investigation. **Addmore Shonhai:** Validation, Resources, Investigation. **Baji Baba Shaik:** Writing – review & editing, Formal analysis. **Ofentse J. Pooe:** Writing – review & editing, Validation, Resources, Formal analysis.

Declaration of competing interest

The authors declare that they have no known conflicting financial or personal interests that could have appeared to influence the work reported in this paper.

Data availability

Data will be made available on request.

Acknowledgement

The authors would like to express the heartflet gratitude to the Discipline of Pharmaceutical Sciences, College of Health Sciences, University of KwaZulu-Natal (UKZN), Durban, South Africa, for providing all the necessary facilities. The authors gratefully acknowledge the National Research Foundation-South Africa (NRF-SA) for funding this project (grant numbers: 103728, 112079 and 129247) awarded to R. Karpoormath., (grant numbers 75464 and 92598) awarded to A. Shonhai. and grant numbers (129401 and 145405) awarded to T. Zininga. The authors would like to acknowledge the NRF-SA (grant number: 112980 and 145396) and the SAMRC-EIP for funding awarded to O. Pooe. Furthermore the authors acknowledge the Mulungushi University research grant awarded F. Kayamba. The authors would also like to acknowledge Dr. Vuyisa Mzozoyana (UKZN) and Thendo P. Mudau for NMR and SPR spectroscopic experimental data. R.L.Van.Zyl., S.L. would like to acknowledge the funding from WITS Faculty of Health Sciences Research Office.

Appendix A. Supplementary data

Supplementary data to this article can be found online at https://doi.org/10.1016/j.ejmech.2024.116944.

References

[1] P. Jagannathan, A. Kakuru, Malaria in 2022: increasing challenges, cautious optimism, Nat. Commun. 13 (2022) 2678.
[2] W.H. Organization, World Malaria Report 2022, World Health Organization, 2022.
[3] F.H. Nosten, A.P. Phyo, New malaria maps, Lancet 394 (2019) 278–279.
[4] R. Who, High Burden to High Impact: a Targeted Malaria Response, World Health Organization, Geneva, 2019.
[5] M.B. Laurens, RTS, S/AS01 vaccine (Mosquirix™): an overview, Hum. Vaccines Immunother. 16 (2020) 480–489.
[6] F. Kayamba, M. Faya, O.J. Pooe, B. Kushwaha, N.D. Kushwaha, V.A. Obakachi, V. O. Nyamori, R. Karpoormath, Lactate dehydrogenase and malate dehydrogenase: potential antiparasitic targets for drug development studies, Bioorg. Med. Chem. 50 (2021) 116458.
[7] L.E. Buyon, B. Elsworth, M.T. Duraisingh, The molecular basis of antimalarial drug resistance in Plasmodium vivax, Int J Parasitol Drugs Drug Resist 16 (2021) 23–37.
[8] J.J. Vanden Eynde, A.A. Mangoni, J. Rautio, J. Leprince, Y.T. Azuma, A.T. García-Sosa, C. Hulme, J. Jampilek, R. Karaman, W. Li, P.A.C. Gomes, D. Hadjipavlou-Litina, R. Capasso, A. Geronikaki, L. Cerchia, J.M. Sabatier, R. Ragno, T. Tuccinardi, A. Trabocchi, J.Y. Winum, F.J. Luque, K. Prokai-Tatrai, M. Spetea, M. Gütschow, I. Kosalec, C. Guillou, M.H. Vasconcelos, G. Kokotos, G. Rastelli, M. E. de Sousa, C. Manera, S. Gemma, S. Mangani, C. Siciliano, S. Galdiero, H. Liu, P.J. H. Scott, C. de Los Ríos, L.A. Agrofoglio, S. Collina, R.C. Guedes, D. Muñoz-Torrero, Breakthroughs in medicinal chemistry: new targets and mechanisms, new drugs, new hopes-6, Molecules 25 (2019).
[9] A.M. Ganai, T.K. Pathan, S.R. Merugu, K. Kozlanská, V. Vojáčková, V. Kryštof, S. Mokoena, F. Kayamba, R. Karpoormath, Development of pyrimidine-cinnamamide hybrids as potential anticancer agents: a rational design approach, J. Mol. Struct. 1267 (2022) 133594.
[10] F. Kayamba, T. Malimabe, I.K. Ademola, O.J. Pooe, N.D. Kushwaha, M. Mahlalela, R.L. van Zyl, M. Gordon, P.T. Mudau, T. Zininga, A. Shonhai, V.O. Nyamori, R. Karpoormath, Design and synthesis of quinoline-pyrimidine inspired hybrids as potential plasmodial inhibitors, Eur. J. Med. Chem. 217 (2021) 113330.
[11] A. Amalraj, A. Pius, S. Gopi, S. Gopi, Biological activities of curcuminoids, other biomolecules from turmeric and their derivatives - a review, J Tradit Complement Med 7 (2017) 205–233.
[12] M.H. Teiten, M. Dicato, M. Diederich, Hybrid curcumin compounds: a new strategy for cancer treatment, Molecules 19 (2014) 20839–20863.
[13] R.C. Reddy, P.G. Vatsala, V.G. Keshamouni, G. Padmanaban, P.N. Rangarajan, Curcumin for malaria therapy, Biochem. Biophys. Res. Commun. 326 (2005) 472–474.

[14] C. Sharma, R. Kumar, A. Sharma, D. Sharma, T. Madhuri, Turmeric (Curcuma longa) WSR to curcumin, World J. Pharmaceut. Res. 6 (2017) 740–753.
[15] Z.D. Wang, Q. Elliott, Z. Wang, R.A. Setien, J. Puttkammer, A. Ugrinov, J. Lee, D. C. Webster, Q.R. Chu, Furfural-derived diacid prepared by photoreaction for sustainable materials synthesis, ACS Sustain. Chem. Eng. 6 (2018) 8136–8141.
[16] L.E. Wright, J.B. Frye, B. Gorti, B.N. Timmermann, J.L. Funk, Bioactivity of turmeric-derived curcuminoids and related metabolites in breast cancer, Curr. Pharmaceut. Des. 19 (2013) 6218–6225.
[17] H. Hatcher, R. Planalp, J. Cho, F.M. Torti, S.V. Torti, Curcumin: from ancient medicine to current clinical trials, Cell. Mol. Life Sci. 65 (2008) 1631–1652.
[18] B. Pérez, C. Teixeira, J. Gut, P.J. Rosenthal, J.R. Gomes, P. Gomes, Cinnamic acid/chloroquinoline conjugates as potent agents against chloroquine-resistant Plasmodium falciparum, ChemMedChem 7 (2012) 1537–1540.
[19] L.L. Franco, M.V. de Almeida, E.S. Lf, P.P. Vieira, A.M. Pohlit, M.S. Valle, Synthesis and antimalarial activity of dihydroperoxides and tetraoxanes conjugated with bis (benzyl)acetone derivatives, Chem. Biol. Drug Des. 79 (2012) 790–797.
[20] M. Larsen, H. Kromann, A. Kharazmi, S.F. Nielsen, Conformationally restricted anti-plasmodial chalcones, Bioorg. Med. Chem. Lett 15 (2005) 4858–4861.
[21] H.B. Rasmussen, S.B. Christensen, L.P. Kvist, A. Karazmi, A simple and efficient separation of the curcumins, the antiprotozoal constituents of Curcuma longa, Planta Med. 66 (2000) 396–398.
[22] K.V. Sashidhara, M. Kumar, R.K. Modukuri, R.K. Srivastava, A. Soni, K. Srivastava, S.V. Singh, J.K. Saxena, H.M. Gauniyal, S.K. Puri, Antiplasmodial activity of novel keto-enamine chalcone-chloroquine based hybrid pharmacophores, Bioorg. Med. Chem. 20 (2012) 2971–2981.
[23] R. Pasupureddy, S. Verma, A. Pant, R. Sharma, S. Seshadri, V. Pande, A.K. Saxena, R. Dixit, K.C. Pandey, Crucial residues in falcipains that mediate hemoglobin hydrolysis, Exp. Parasitol. 197 (2019) 43–50.
[24] B. Pradines, C. Rogier, T. Fusai, J. Mosnier, W. Daries, E. Barret, D. Parzy, In vitro activities of antibiotics against Plasmodium falciparum are inhibited by iron, Antimicrob. Agents Chemother. 45 (2001) 1746–1750.
[25] N. Rastogi, K.S. Goh, L. Horgen, W.W. Barrow, Synergistic activities of antituberculous drugs with cerulenin and trans-cinnamic acid against Mycobacterium tuberculosis, FEMS Immunol. Med. Microbiol. 21 (1998) 149–157.
[26] X. Nqoro, N. Tobeka, B.A. Aderibigbe, Quinoline-based hybrid compounds with antimalarial activity, Molecules 22 (2017).
[27] J.A. Badejo, O.O. Abiodun, O. Akinola, C.T. Happi, A. Sowunmi, G.O. Gbotosho, Interaction between rifampicin, amodiaquine and artemether in mice infected with chloroquine resistant Plasmodium berghei, Malar. J. 13 (2014) 299.
[28] M. Strath, T. Scott-Finnigan, M. Gardner, D. Williamson, I. Wilson, Antimalarial activity of rifampicin in vitro and in rodent models, Trans. R. Soc. Trop. Med. Hyg. 87 (1993) 211–216.
[29] S. Manohar, U.C. Rajesh, S.I. Khan, B.L. Tekwani, D.S. Rawat, Novel 4-aminoquinoline-pyrimidine based hybrids with improved in vitro and in vivo antimalarial activity, ACS Med. Chem. Lett. 3 (2012) 555–559.
[30] F. Kayamba, T. Malimabe, I.K. Ademola, O.J. Pooe, N.D. Kushwaha, M. Mahlalela, R.L. van Zyl, M. Gordon, P.T. Mudau, T. Zininga, A. Shonhai, V.O. Nyamori, R. Karpoormath, Design and synthesis of quinoline-pyrimidine inspired hybrids as potential plasmodial inhibitors, Eur. J. Med. Chem. 217 (2021) 113330.
[31] D. Giles, K. Roopa, F.R. Sheeba, P.M. Gurubasavarajaswamy, G. Divakar, T. Vidhya, Synthesis pharmacological evaluation and docking studies of pyrimidine derivatives, Eur. J. Med. Chem. 58 (2012) 478–484.
[32] J. Dickson, L. Flores, M. Stewart, R. LeBlanc, H.N. Pati, M. Lee, H. Holt, Synthesis and cytotoxic properties of chalcones: an interactive and investigative undergraduate laboratory project at the interface of chemistry and Biology, J. Chem. Educ. 83 (2006) 934.
[33] B. Burger, An Aldol Condensation to Synthesize Chalcones. Website: https://cpb-us-e1.wpmucdn.com/sites.psu.edu/dist/a/25494/files/2015/04/An-Aldol-Condensation-to-synthesize-Chalcones.pdf.
[34] A. Ganeshpurkar, D. Kumar, S.K. Singh, Strategies for the synthesis of hydroxamic acids, Curr. Org. Synth. 15 (2018) 154–165.
[35] A.D. Forkuo, C. Ansah, K.B. Mensah, K. Annan, B. Gyan, A. Theron, D. Mancama, C. W. Wright, In vitro anti-malarial interaction and gametocytocidal activity of cryptolepine, Malar. J. 16 (2017) 496.
[36] L.G. Ferreira, R.N. Dos Santos, G. Oliva, A.D. Andricopulo, Molecular docking and structure-based drug design strategies, Molecules 20 (2015) 13384–13421.
[37] H. Guterres, W. Im, Improving protein-ligand docking results with high-throughput molecular dynamics simulations, J. Chem. Inf. Model. 60 (2020) 2189–2198.
[38] I. Kehinde, P. Ramharack, M. Nlooto, M. Gordon, The pharmacokinetic properties of HIV-1 protease inhibitors: a computational perspective on herbal phytochemicals, Heliyon 5 (2019) e02565.
[39] A.T. Adewumi, O.S. Soremekun, M.B. Ajadi, M.E. Soliman, Thompson loop: opportunities for antitubercular drug design by targeting the weak spot in demethylmenaquinone methyltransferase protein, RSC Adv. 10 (2020) 23466–23483.
[40] O.I. Akinpelu, M.M. Lawal, H.M. Kumalo, N.N. Mhlongo, Drug repurposing: fusidic acid as a potential inhibitor of M. tuberculosis FtsZ polymerization – insight from DFT calculations, molecular docking and molecular dynamics simulations, Tuberculosis 121 (2020) 101920.
[41] S.E. Boyce, N. Tirunagari, A. Niedziela-Majka, J. Perry, M. Wong, E. Kan, L. Lagpacan, O. Barauskas, M. Hung, M. Fenaux, Structural and regulatory elements of HCV NS5B polymerase–β-loop and C-terminal tail–are required for activity of allosteric thumb site II inhibitors, PLoS One 9 (2014) e84808.
[42] D.J. Begley, M.W. Brightman, Structural and Functional Aspects of the Blood-Brain Barrier, Peptide Transport and Delivery into the Central Nervous System, 2003, pp. 39–78.
[43] C.A. Lipinski, F. Lombardo, B.W. Dominy, P.J. Feeney, Experimental and computational approaches to estimate solubility and permeability in drug discovery and development settings, Adv. Drug Deliv. Rev. 23 (1997) 3–25.
[44] M. Remko, A. Boháč, L. Kováčiková, Molecular structure, pKa, lipophilicity, solubility, absorption, polar surface area, and blood brain barrier penetration of some antiangiogenic agents, Struct. Chem. 22 (2011) 635–648.
[45] C. Lambros, J.P. Vanderberg, Synchronization of plasmodium falciparum erythrocytic stages in culture, J. Parasitol. 65 (1979) 418–420.
[46] M.T. Makler, J.M. Ries, J.A. Williams, J.E. Bancroft, R.C. Piper, B.L. Gibbins, D. J. Hinrichs, Parasite lactate dehydrogenase as an assay for Plasmodium falciparum drug sensitivity, Am. J. Trop. Med. Hyg. 48 (1993) 739–741.
[47] J. Reader, M. Botha, A. Theron, S.B. Lauterbach, C. Rossouw, D. Engelbrecht, M. Wepener, A. Smit, D. Leroy, D. Mancama, T.L. Coetzer, L.-M. Birkholtz, Nowhere to hide: interrogating different metabolic parameters of Plasmodium falciparum gametocytes in a transmission blocking drug discovery pipeline towards malaria elimination, Malar. J. 14 (2015) 213.
[48] T. Mosmann, Rapid colorimetric assay for cellular growth and survival: application to proliferation and cytotoxicity assays, Journal of Immunological Methods 65 (1983).
[49] J.C. Domingue, M. Ao, J. Sarathy, A. George, W.A. Alrefai, D.J. Nelson, M.C. Rao, HEK-293 cells expressing the cystic fibrosis transmembrane conductance regulator (CFTR): a model for studying regulation of Cl− transport, Physiological reports 2 (2014) e12158.
[50] K.M. Krawczyk, D. Matak, L. Szymanski, C. Szczylik, C. Porta, A.M. Czarnecka, Culture in embryonic kidney serum and xeno-free media as renal cell carcinoma and renal cell carcinoma cancer stem cells research model, Cytotechnology 70 (2018).
[51] F. Hayat, E. Moseley, A. Salahuddin, R.L. Van Zyl, A. Azam, Antiprotozoal activity of chloroquinoline based chalcones, Eur. J. Med. Chem. 46 (2011) 1897–1905.
[52] T. Zininga, S. Makumire, G.W. Gitau, J.M. Njunge, O.J. Pooe, H. Klimek, R. Scheurr, H. Raifer, E. Prinsloo, J.M. Przyborski, Plasmodium falciparum Hop (PfHop) interacts with the Hsp70 chaperone in a nucleotide-dependent fashion and exhibits ligand selectivity, PLoS One 10 (2015) e0135326.
[53] T. Zininga, O.J. Pooe, P.B. Makhado, L. Ramatsui, E. Prinsloo, I. Achilonu, H. Dirr, A. Shonhai, Polymyxin B inhibits the chaperone activity of Plasmodium falciparum Hsp70, Cell Stress & Chaperones 22 (2017) 707–715.
[54] A. Waterhouse, M. Bertoni, S. Bienert, G. Studer, G. Tauriello, R. Gumienny, F. T. Heer, T.A.P. de Beer, C. Rempfer, L. Bordoli, R. Lepore, T. Schwede, SWISS-MODEL: homology modelling of protein structures and complexes, Nucleic Acids Res. 46 (2018) W296–W303.
[55] M.D. Hanwell, D.E. Curtis, D.C. Lonie, T. Vandermeersch, E. Zurek, G.R. Hutchison, Avogadro: an advanced semantic chemical editor, visualization, and analysis platform, J. Cheminf. 4 (2012) 17.
[56] A. Grosdidier, V. Zoete, O. Michielin, SwissDock, a protein-small molecule docking web service based on EADock DSS, Nucleic Acids Res. 39 (2011) W270–W277.
[57] O. Trott, A.J. Olson, AutoDock Vina: improving the speed and accuracy of docking with a new scoring function, efficient optimization, and multithreading, J. Comput. Chem. 31 (2010) 455–461.
[58] L. Shunmugam, M.E. Soliman, Targeting HCV polymerase: a structural and dynamic perspective into the mechanism of selective covalent inhibition, RSC Adv. 8 (2018) 42210–42222.
[59] J.-P. Ryckaert, G. Ciccotti, H.J.C. Berendsen, Numerical integration of the cartesian equations of motion of a system with constraints: molecular dynamics of n-alkanes, J. Comput. Phys. 23 (1977) 327–341.
[60] O.S. Soremekun, F.A. Olotu, C. Agoni, M.E.S. Soliman, Recruiting monomer for dimer formation: resolving the antagonistic mechanisms of novel immune check point inhibitors against Programmed Death Ligand-1 in cancer immunotherapy, Mol. Simulat. 45 (2019) 777–789.
[61] U. Kalathiya, M. Padariya, M. Baginski, Structural, functional, and stability change predictions in human telomerase upon specific point mutations, Sci. Rep. 9 (2019) 8707.
[62] W. Humphrey, A. Dalke, K. Schulten, VMD: visual molecular dynamics, J. Mol. Graph. 14 (1996) 33–38.
[63] E. Seifert, OriginPro 9.1: scientific data analysis and graphing software-software review, J. Chem. Inf. Model. 54 (2014) 1552.
[64] M. Ylilauri, O.T. Pentikäinen, MMGBSA as a tool to understand the binding affinities of filamin–peptide interactions, J. Chem. Inf. Model. 53 (2013) 2626–2633.